


2008

Mesoporous silica nanomaterials and magnetic nanoparticles based stimuli-responsive controlled-release delivery systems

Supratim Giri
Iowa State University

Follow this and additional works at: <https://lib.dr.iastate.edu/rtd>

 Part of the [Chemical and Pharmacologic Phenomena Commons](#), [Inorganic Chemistry Commons](#), [Medicinal and Pharmaceutical Chemistry Commons](#), [Medicinal Chemistry and Pharmaceutics Commons](#), and the [Medicinal-Pharmaceutical Chemistry Commons](#)

Recommended Citation

Giri, Supratim, "Mesoporous silica nanomaterials and magnetic nanoparticles based stimuli-responsive controlled-release delivery systems" (2008). *Retrospective Theses and Dissertations*. 15769.
<https://lib.dr.iastate.edu/rtd/15769>

This Dissertation is brought to you for free and open access by the Iowa State University Capstones, Theses and Dissertations at Iowa State University Digital Repository. It has been accepted for inclusion in Retrospective Theses and Dissertations by an authorized administrator of Iowa State University Digital Repository. For more information, please contact digirep@iastate.edu.

Mesoporous silica nanomaterials and magnetic nanoparticles based stimuli-responsive controlled-release delivery systems

by

Supratim Giri

A dissertation submitted to the graduate faculty
in partial fulfillment of the requirements for the degree of
DOCTOR OF PHILOSOPHY

Major: Chemistry

Program of Study Committee:
Victor S. -Y. Lin, Major Professor
Nicola L. Pohl
Marek Pruski
Aaron D. Sadow
L. Keith Woo

Iowa State University

Ames, Iowa

2008

UMI Number: 3337380

INFORMATION TO USERS

The quality of this reproduction is dependent upon the quality of the copy submitted. Broken or indistinct print, colored or poor quality illustrations and photographs, print bleed-through, substandard margins, and improper alignment can adversely affect reproduction.

In the unlikely event that the author did not send a complete manuscript and there are missing pages, these will be noted. Also, if unauthorized copyright material had to be removed, a note will indicate the deletion.



UMI Microform 3337380
Copyright 2009 by ProQuest LLC
All rights reserved. This microform edition is protected against
unauthorized copying under Title 17, United States Code.

ProQuest LLC
789 East Eisenhower Parkway
P.O. Box 1346
Ann Arbor, MI 48106-1346

TABLE OF CONTENTS

ABSTRACT.....	iii
CHAPTER 1. GENERAL INTRODUCTION	1
Dissertation organization	1
Introduction.....	1
References.....	9
CHAPTER 2. STIMULI-RESPONSIVE CONTROLLED-RELEASE DELIVERY SYSTEM BASED ON MESOPOROUS SILICA NANORODS CAPPED WITH MAGNETIC NANOPARTICLES.....	14
Abstract.....	14
Introduction.....	14
Results and discussion	17
Conclusion	25
Experimental section.....	25
References.....	28
Appendix.....	32
CHAPTER 3. INHIBITION OF GROWTH OF HUMAN CERVICAL CANCER CELL LINE (HeLa) BY INTRACELLULAR RELEASE OF A DNA- INTERCALATING DRUG FROM MAGNETIC NANOPARTICLE CAPPED MESOPOROUS SILICA NANORODS	37
Abstract.....	37
Introduction.....	37
Results and discussions.....	39
Conclusion	44
Experimental section.....	45
References.....	46
CHAPTER 4. A MAGNETIC NANOPARTICLE ATTACHED PNIPAM POLYMER COATED MESOPOROUS SILICA NANOPARTICLE BASED HEAT RESPONSIVE DELIVERY SYSTEM USING ALTERNATING MAGNETIC FIELD AS STIMULI	48
Abstract.....	48
Introduction.....	48
Results and discussion	51
Conclusion	65
Experimental section.....	66
References.....	70
CHAPTER 5. GENERAL CONCLUSION	73

ABSTRACT

The research presented and discussed within this dissertation involves the development of mesoporous silica nanomaterials and magnetic nanoparticles based stimuli-responsive controlled-release delivery systems.

A superparamagnetic iron oxide nanoparticle-capped, MCM-41 type mesoporous silica nanorod-based controlled-release delivery system (Magnet-MSN) was synthesized. The stimuli-responsive release profiles of fluorescein-loaded Magnet-MSN delivery systems in the presence of external magnetic field was studied by using cell-produced antioxidants as triggers for releasing fluorescein molecules. The intracellular delivery efficiency of the Magnet-MSN system with human cervical cancer cells (HeLa) *in vitro* was demonstrated involving fluorescein molecules as model drug.

To take the advantage of the intracellular delivery capability of Magnet-MSN systems, a series of *in vitro* experiments demonstrating the loading and release of a DNA intercalating drug 9-aminoacridine was performed using Magnet-MSN by the action of reductant triggers. The *in vivo* application of Magnet-MSN with HeLa cells led to the enhanced cell growth inhibition effect. The cell growth inhibition was found to be unaffected by a strong external magnetic field.

A poly(*N*-isopropylacrylamide) coated mesoporous silica nanomaterials (PNiPAm-MSN) was demonstrated to load and release drug molecules using thermal stimuli as a trigger. Iron oxide (Fe₃O₄) nanoparticles were then attached to the surface of drug loaded PNiPAm-MSN to render the system magnetic (Mag-PNiPAm-MSN). Successful release of

the loaded drug molecules was shown by placing Mag-PNiPAm-MSN under an alternating current based magnetic field. The mechanism of drug release was explained by the action of hyperthermia effect originating from the attached magnetic nanoparticles under the high frequency alternating magnetic field. The rate of drug release was also shown to be precisely controllable by controlling the parameters of the external magnetic field.

CHAPTER 1. GENERAL INTRODUCTION

Dissertation organization

The dissertation starts with Chapter 1, which is a general introduction about the aspects of mesoporous silica nanomaterials as controlled-release delivery agents. Some of the important biomedical applications of mesoporous silica materials are also discussed briefly. Chapter 2 involves the description of the development of a novel stimuli-responsive, controlled-release delivery system based on mesoporous silica nanorods capped with magnetic nanoparticles. A successful intracellular delivery of a fluorescent dye by the action of a cell produced anti-oxidant is also reported here. Chapter 3 describes the effect of growth inhibition of a cancer cell line upon introduction of magnetic nanoparticle-capped silica nanorods loaded with a mutagenic drug and the influence of magnetic field on the cell growth. A novel concept of magnetic field induced controlled-release delivery system is reported in Chapter 4 by using a thermo-responsive polymer coated mesoporous silica nanomaterial attached with magnetic nanoparticles. In this chapter, the controlled-release of a mutagenic drug is demonstrated by manipulating the alternating current associated with the induced magnetic field. Finally in Chapter 5, the significance and future prospect of the research done in this dissertation is discussed as a general conclusion.

Introduction

For many biomedical applications, an ideal delivery system should have the ability to deliver a large amount of guest molecules to a targeted site and release the cargo in a

controllable fashion.¹ However, in many current liposome- and polymer-based delivery systems, guest molecules are often released upon dispersion of the carrier/drug composites in water.²⁻⁴ This kind of premature release is particularly undesirable and problematic when the guest molecules, e.g., antitumor drugs, are cytotoxic and can potentially harm healthy cells and tissues before being delivered to affected sites. Therefore, a desired biomedical delivery system should have the following features:

1. Biocompatibility.
2. Capability of loading and releasing a large quantity of guest molecules, such as pharmaceutical drugs, genes, and nutrients.
3. Controllable rate of release.
4. Stimuli responsive property.
5. Site specificity.

To introduce these features to biocompatible materials, many research groups worldwide have focused on designing new chemical strategies^{5,6} for the synthesis of hybrid organic-inorganic nanomaterials.⁷ In particular, recent advancements in the synthesis of hybrid organic-inorganic nanomaterials, such as carbon nanotubes, dendrimers and mesoporous metal oxides, have greatly improved their biocompatibility. The utilization of these structurally well defined nanoporous materials for controlled release delivery applications for pharmaceutical drugs,⁸⁻¹⁰ biocides, genes and proteins¹¹⁻¹⁵ in vitro and/or in vivo has become global pursuit.

Mesoporous silica materials, such as MCM-41/48,^{16,17} SBA-15,¹⁸ MSU-n,¹⁹ KIT-1,²⁰ and FSM-16²¹ can be synthesized by utilizing surfactants as structure-directing templates to generate a range of mesoporous structures with high surface area ($> 900 \text{ m}^2/\text{g}$), tunable pore

size (2 to 20 nm), and uniform pore morphology (hexagonal channels and cubic pores). These unique features offer immense potential for various biomedical delivery applications. The quantity of host molecules that can be encapsulated by the ordered mesoporous silica nanomaterials due to their high surface area and large pore volume, is almost comparable with the drug loading capacity of conventional drug delivery agents such as polymeric or liposomal nanoparticles.²²⁻²⁸ However, the real advantage of mesoporous silica nanomaterial lies in the chemically inert nature of silica, which enables the material to store a wide range of biomolecules without chemical modification. In contrast, many of the bio-degradable polymeric drug delivery systems require organic solvents for the loading of drug molecules and drug release mechanism rely on the hydrolysis-induced erosion of the carrier structure for drug delivery and this leads to the undesirable structural or functional modifications or both of the encapsulated molecules.²⁹⁻³¹ Also, some of the conventional drug delivery agents such as liposomal nanoparticles, break down once these are trapped on cell surface and drugs simply leak out and traverse the plasma membrane by diffusion or pore formation.³² Alternatively, the liposomes may either directly fuse with plasma membrane, or they may be taken up by endocytosis or phagocytosis. Therefore, these types of conventional drug delivery vehicles lack of control. On the other hand, well ordered mesoporous silica nanomaterials when equipped with removable caps overcome this undesired drug leaching problem. However, mesoporous silicas with amorphous particle morphology typically show insufficient biocompatibility with various cell types. In contrast to the abundant literature reports on applying micron-sized, colloidal silica particles to biotechnological and biomedical applications, the cell growth and differentiation processes of mammalian cells were shown to be hindered upon introduction of the as-synthesized mesoporous silicas with

amorphous particle morphology.^{33,34} The origin of this low biocompatibility has been attributed to the cytotoxicity of the residual surfactant³⁵⁻³⁷ template and the amorphous mesoporous silica particles with small sizes (<10 nm) that are often hydrolyzed in aqueous solution forming high concentrations of silicic acid.^{33,38-40}

Unlike the amorphous mesoporous silicas, the Lin group as well as the others have recently developed new synthetic methods for preparing monodisperse, organically functionalized mesoporous silica nanoparticle (MSN) materials^{41,42} that are highly biocompatible.^{34,43-45} By using these biocompatible MSNs as carriers, several controlled release drug delivery systems have been developed. In this chapter, I discuss some of the unique utilities of mesoporous silica nanomaterials in the field of biomedical application very briefly.

Mesoporous silica nanomaterials as delivery agents:

Stable mesoporous structures, large surface areas, tunable pore sizes and volumes, and well defined surface properties of the MCM-type mesoporous silica materials have made them ideal for hosting wide varieties of biomolecules having various shapes, sizes and functionalities. Over the past five years, there have been several examples of these MCM-type materials used for drug delivery and controlled release. For example, Vallet-Regí and coworkers¹⁰ showed that it was possible to fill the mesopores of MCM-41 material with a drug and release the drug at a later time. The researchers loaded ibuprofen into two MCM-41 materials with different pore sizes and studied the release in a simulated body fluid. This work was the first demonstration on the utilization of non-functionalized MCM-41 silicas with different pore structures for controlled release applications. Similar studies of the

loading of ibuprofen and controlled release of the same in simulated body fluid involving MCM-41 was also reported by Devoisselle and co-workers.⁴⁶

The morphology of mesoporous silica materials has a defining role on controlled release of encapsulated molecules was also emphasized in one of the recent reports on the synthesis, characterization, and application of room temperature ionic liquid (RTIL) templated mesoporous silica nanoparticles published by our research group.⁴⁷ By using 4 different RTILs as templates, Trewyn et al. synthesized a series of RTIL-MSN materials with various particle morphologies including spheres, ellipsoids, rods, and tubes. By changing the RTIL template, the pore morphologies were tuned from the MCM-41 type of hexagonal mesopores to rotational moiré type of helical channels, and to wormhole-like porous structures. Followed by the synthesis and the full characterization of these materials, Trewyn et al. investigated the controlled diffusion of RTILs from the pores by measuring the antibacterial effect on *Escherichia coli* K12. The antibacterial activities of two RTIL-MSNs, one spherical with hexagonal mesopores and the other tubular with wormhole mesopores, at 37 °C in *E. coli* cultures were measured. While both the RTILs displayed very similar antibacterial activities, the spherical, hexagonally mesopore RTIL-MSN exhibited a superior antibacterial activity to that of the tubular, wormhole RTIL-MSN by 1000-fold. The result was attributed to the fact that the rate of RTIL release via diffusion from the parallel hexagonal channels would be faster than that of the disordered wormhole pores. Also understandably, the mass transfer from the tubular particles would be considerably slower than in the case of spherical particles. This work categorically demonstrated the essential role of the morphology of mesoporous silica nanomaterials on controlled release behavior.

To further control the release profiles, many have been investigating the controlled release of guest molecules from organic modifier functionalized MCM-41 capped with various organic and inorganic blockades. For example, Tanaka and coworkers demonstrated the ability of coumarin-modified mesoporous silica being used as a photocontrolled reversible guest molecule release vehicle.⁴⁸ They showed that the uptake, storage, and release of organic molecules using coumarin-modified MCM-41 can be regulated through the photocontrolled and reversible intermolecular dimerization. The coumarin was covalently attached with the MCM-41 pore walls by post synthesis grafting and the pores were loaded with the steroid cholestane followed by photodimerization of the coumarin by exposure to wavelengths greater than 310 nm. The resulting photodimerization led to the isolation of pores by blocking the pore entrance with cyclobutane dimers spanning the pore diameter. The cholestane loaded photodimerized material was then exposed to UV light with a wavelength of 250 nm to cleave the cyclobutane rings of the coumarin dimers and the subsequent release of the stored cholestane molecules was observed. The publication was the first to demonstrate a photocontrolled release of guest molecules from MCM-41 material by reversible photo responsive dimerization techniques.

Also, our research group has demonstrated that large organic molecules can modify the surface charge property of MCM-41 silicas to further manipulate the controlled release profiles.³⁴ The study published by Radu et al. detailed the synthesis of thiol functionalized MCM-41, and the covalent attachment of second generation (G2) PAMAM dendrimer to the surface of a MCM-41 type mesoporous silica nanosphere (MSN). The G2-PAMAM-capped MSN (G2-MSN) was used to complex with plasmid DNA (pEGFP-C1) that codes for enhanced green fluorescent protein. Following, Radu et al. investigated the gene transfection

efficacy, uptake mechanism, and biocompatibility of the G2-MSN with astrocytes, human cervical cancer (HeLa), and Chinese hamster ovarian (CHO) cells. It was determined that the G2-MSN could bind with plasmid DNA to form stable DNA-MSN complexes at weight ratios larger than 1:5 through agarose gel electrophoresis. They also showed that this DNA-MSN complex protects the plasmid DNA from enzymatic cleavage too. This was demonstrated by introducing the complex to a restriction endonuclease at varying weight ratios. Transfection efficacy was demonstrated by incubating the DNA-MSN complex with cells and measuring the expression of GFP by flow cytometry. Fluorescence confocal microscopy clearly illustrated that the G2-MSN, entered the cytoplasm of neural glia cells. Transmission electron micrographs of post-transfection cells also provided direct evidence that a large number of G2-MSN-DNA complexes were endocytosed by all those three types of cells.

Besides the dendrimer based soft capping systems described before, some inorganic nanoparticles used as “hard caps” also offer a series of MCM-41 type novel drug carrier systems. The characteristic chemical or physical nature of those inorganic nanoparticles can be of added advantage to make these kinds of controlled release delivery systems more versatile and prospective. Our group developed a MCM-41 type mesoporous silica-based controlled release delivery system where loaded guest molecules inside the host mesoporous silica material were capped by CdS nanoparticles.⁴⁵ Being physically blocked, guest molecules were unable to come out from the host, thus preventing any premature release and the system was designed in such a way that the release could occur in a controlled manner only when the caps were taken off by external chemical stimuli. Although, this system fulfills the “zero release” pre-requisite for targeted drug delivery application, it does lack any

inherent site directing capability. In recent times, a great deal of research interest has been focused towards the development of a mesoporous silica based site specific delivery systems. Often times the common approach of introduction of the site specificity or the targeting ability of the delivery system has been achieved by incorporating magnetic nanoparticles within the system. A majority of such systems are developed based on a mesoporous silica shell having a core of magnetic nanoparticle.⁴⁹⁻⁵¹ In such reported systems, drugs can be either loaded or a fluorescent marker molecule can be covalently attached in the silica shell. As the core of these systems consists of magnetic nanoparticles, the entire delivery system can be guided to a specific site of interest using a magnetic field. However these kind of core-shell materials suffer from a serious drawback. The drugs can potentially leach out from the uncapped silica shells as soon as the drug loaded system is dispersed into physiological media. Therefore the lack of “zero release” criteria limit the application of this silica shell-magnetic core based systems to a great extent. Hence the development of a controlled release delivery system, which is stimuli responsive and has a targeting ability, is immensely important. In this context, a few novel nanomaterial-based delivery systems have been developed in our laboratory and those are the primary topics of this doctoral dissertation.

Even though the long-term in vivo biocompatibility has not been determined yet, the aforementioned reports in the literature have shown promising potential in using these materials for in vitro drug/gene delivery. In particular, the efficiency of cellular uptake of the capped-MSN systems offers the possibility of utilizing these stimuli-responsive, controlled release systems to investigate various intracellular chemical/neurochemical communications. Also, it is foreseeable that more functionalized mesoporous silica nanomaterials with surface moieties, such as peptides, proteins, antibodies, and carbohydrates, that can regulate the

properties of in vivo circulation and serve as site-directing agents would be developed. Further efforts in manipulating the porous structure, such as pore expansion, would also enable the encapsulation of biological macromolecules, such as enzymes and genes, which could lead to delivery systems for gastro- and intestinal applications.

References

- (1) Giri, S.; Trewyn, B. G.; Lin, V. S. Y. *Nanomedicine (London, United Kingdom)* **2007**, *2*, 99-111.
- (2) Aughenbaugh, W.; Radin, S.; Ducheyne, P. *Journal of Biomedical Materials Research* **2001**, *57*, 321-326.
- (3) Korteso, P.; Ahola, M.; Kangas, M.; Kangasniemi, I.; Yli-Urpo, A.; Kiesvaara, J. *International journal of pharmaceutics* **2000**, *200*, 223-9.
- (4) Radin, S.; Ducheyne, P.; Kamplain, T.; Tan, B. H. *Journal of biomedical materials research* **2001**, *57*, 313-20.
- (5) de Soler-Illia, G. J.; Sanchez, C.; Lebeau, B.; Patarin, J. *Chemical Reviews (Washington, DC, United States)* **2002**, *102*, 4093-4138.
- (6) Sanchez, C.; Arribart, H.; Madeleine, M.; Guille, G. *Nature Materials* **2005**, *4*, 277-288.
- (7) Sanchez, C.; Julian, B.; Belleville, P.; Popall, M. *Journal of Materials Chemistry* **2005**, *15*, 3559-3592.
- (8) Munoz, B.; Ramila, A.; Perez-Pariente, J.; Diaz, I.; Vallet-Regi, M. *Chemistry of Materials* **2003**, *15*, 500-503.

- (9) Ramila, A.; Munoz, B.; Perez-Pariente, J.; Vallet-Regi, M. *Journal of Sol-Gel Science and Technology* **2003**, *26*, 1199-1202.
- (10) Vallet-Regi, M.; Ramila, A.; del Real, R. P.; Perez-Pariente, J. *Chemistry of Materials* **2001**, *13*, 308-311.
- (11) Diaz, J. F.; Balkus, K. J., Jr. *Journal of Molecular Catalysis B: Enzymatic* **1996**, *2*, 115-126.
- (12) Han, Y.-J.; Stucky, G. D.; Butler, A. *Journal of the American Chemical Society* **1999**, *121*, 9897-9898.
- (13) Kisler, J. M.; Dahler, A.; Stevens, G. W.; O'Connor, A. J. *Microporous and Mesoporous Materials* **2001**, *44-45*, 769-774.
- (14) Takahashi, H.; Li, B.; Sasaki, T.; Miyazaki, C.; Kajino, T.; Inagaki, S. *Microporous and Mesoporous Materials* **2001**, *44-45*, 755-762.
- (15) Yiu, H. H. P.; Wright, P. A.; Botting, N. P. *Microporous and Mesoporous Materials* **2001**, *44-45*, 763-768.
- (16) Beck, J. S.; Vartuli, J. C.; Roth, W. J.; Leonowicz, M. E.; Kresge, C. T.; Schmitt, K. D.; Chu, C. T. W.; Olson, D. H.; Sheppard, E. W.; et al. *J. Am. Chem. Soc.* **1992**, *114*, 10834-43.
- (17) Kresge, C. T.; Leonowicz, M. E.; Roth, W. J.; Vartuli, J. C.; Beck, J. S. *Nature (London)* **1992**, *359*, 710-12.
- (18) Zhao, D.; Feng, J.; Huo, Q.; Melosh, N.; Frederickson, G. H.; Chmelka, B. F.; Stucky, G. D. *Science (Washington, D. C.)* **1998**, *279*, 548-552.
- (19) Bagshaw, S. A.; Prouzet, E.; Pinnavaia, T. J. *Science (Washington, D. C.)* **1995**, *269*, 1242-4.

- (20) Ryoo, R.; Kim, J. M.; Ko, C. H.; Shin, C. H. *Journal of Physical Chemistry* **1996**, *100*, 17718-17721.
- (21) Inagaki, S.; Koiwai, A.; Suzuki, N.; Fukushima, Y.; Kuroda, K. *Bulletin of the Chemical Society of Japan* **1996**, *69*, 1449-1457.
- (22) Nasongkla, N.; Shuai, X.; Ai, H.; Weinberg, B. D.; Pink, J.; Boothman, D. A.; Gao, J. *Angewandte Chemie, International Edition* **2004**, *43*, 6323-6327.
- (23) Zeisser-Labouebe, M.; Lange, N.; Gurny, R.; Delie, F. *International Journal of Pharmaceutics* **2006**, *326*, 174-181.
- (24) Nasongkla, N.; Bey, E.; Ren, J.; Ai, H.; Khemtong, C.; Guthi, J. S.; Chin, S.-F.; Sherry, A. D.; Boothman, D. A.; Gao, J. *Nano Letters* **2006**, *6*, 2427-2430.
- (25) Xiao, C.; Qi, X.; Maitani, Y.; Nagai, T. *Journal of Pharmaceutical Sciences* **2004**, *93*, 1718-1724.
- (26) Sezer, A. D.; Bas, A. L.; Akbuga, J. *Journal of Liposome Research* **2004**, *14*, 77-86.
- (27) Anderson, M.; Omri, A. *Drug Delivery* **2004**, *11*, 33-39.
- (28) Gursoy, A.; Kut, E.; Ozkirimli, S. *International Journal of Pharmaceutics* **2004**, *271*, 115-123.
- (29) Uhrich, K. E.; Cannizzaro, S. M.; Langer, R. S.; Shakesheff, K. M. *Chemical Reviews (Washington, D. C.)* **1999**, *99*, 3181-3198.
- (30) Langer, R. *Accounts of Chemical Research* **1993**, *26*, 537-42.
- (31) Li, Y.; Kissel, T. *Journal of Controlled Release* **1993**, *27*, 247-57.
- (32) Ulrich Anne, S. *Bioscience reports* **2002**, *22*, 129-50.
- (33) Fenoglio, I.; Prandi, L.; Tomatis, M.; Fubini, B. *Studies in Surface Science and Catalysis* **2001**, *135*, 5259-5267.

- (34) Radu, D. R.; Lai, C.-Y.; Jeftinija, K.; Rowe, E. W.; Jeftinija, S.; Lin, V. S. Y. *Journal of the American Chemical Society* **2004**, *126*, 13216-13217.
- (35) Benoit, J.; Cormier, M.; Wepierre, J. *Toxicology in Vitro* **1987**, *1*, 91-6.
- (36) Scaife, M. C. *International Journal of Cosmetic Science* **1982**, *4*, 179-94.
- (37) Scaife, M. C. *Food Chem. Toxicol.* **1985**, *23*, 253-8.
- (38) Comolli, R. *J. pathol. bacteriol.* **1967**, *93*, 241-53.
- (39) Kane, A. B.; Stanton, R. P.; Raymond, E. G.; Dobson, M. E.; Knafelc, M. E.; Farber, J. L. *The Journal of cell biology* **1980**, *87*, 643-51.
- (40) Lim, Y.; Kim, J. H.; Kim, K. A.; Chang, H. S.; Park, Y. M.; Ahn, B. Y.; Phee, Y. G. *Toxicol. Lett.* **1999**, *108*, 335-339.
- (41) Huh, S.; Wiench, J. W.; Yoo, J.-C.; Pruski, M.; Lin, V. S. Y. *Chemistry of Materials* **2003**, *15*, 4247-4256.
- (42) Gruenhagen, J. A.; Lai, C.-Y.; Radu, D. R.; Lin, V. S. Y.; Yeung, E. S. *Applied Spectroscopy* **2005**, *59*, 424-431.
- (43) Giri, S.; Trewyn, B. G.; Stellmaker, M. P.; Lin, V. S. Y. *Angewandte Chemie, International Edition* **2005**, *44*, 5038-5044.
- (44) Huang, D.-M.; Hung, Y.; Ko, B.-S.; Hsu, S.-C.; Chen, W.-H.; Chien, C.-L.; Tsai, C.-P.; Kuo, C.-T.; Kang, J.-C.; Yang, C.-S.; Mou, C.-Y.; Chen, Y.-C. *FASEB Journal* **2005**, *19*, 2014-2016.
- (45) Lai, C.-Y.; Trewyn, B. G.; Jeftinija, D. M.; Jeftinija, K.; Xu, S.; Jeftinija, S.; Lin, V. S. Y. *Journal of the American Chemical Society* **2003**, *125*, 4451-4459.
- (46) Charnay, C.; Begu, S.; Tourne-Peteilh, C.; Nicole, L.; Lerner, D. A.; Devoisselle, J. M. *European Journal of Pharmaceutics and Biopharmaceutics* **2004**, *57*, 533-540.

- (47) Trewyn, B. G.; Whitman, C. M.; Lin, V. S. Y. *Nano Letters* **2004**, *4*, 2139-2143.
- (48) Mal, N. K.; Fujiwara, M.; Tanaka, Y. *Nature (London, United Kingdom)* **2003**, *421*, 350-353.
- (49) Yoon, T.-J.; Kim, J. S.; Kim, B. G.; Yu, K. N.; Cho, M.-H.; Lee, J.-K. *Angewandte Chemie, International Edition* **2005**, *44*, 1068-1071.
- (50) Zhao, W.; Gu, J.; Zhang, L.; Chen, H.; Shi, J. *Journal of the American Chemical Society* **2005**, *127*, 8916-8917.
- (51) Lin, Y.-S.; Wu, S.-H.; Hung, Y.; Chou, Y.-H.; Chang, C.; Lin, M.-L.; Tsai, C.-P.; Mou, C.-Y. *Chemistry of Materials* **2006**, *18*, 5170-5172.

CHAPTER 2. STIMULI-RESPONSIVE CONTROLLED-RELEASE DELIVERY SYSTEM BASED ON MESOPOROUS SILICA NANORODS CAPPED WITH MAGNETIC NANOPARTICLES

¹ A paper published in *Angew. Chem. Int. Ed.* **2005**, *44*, 5038-5044.

*Supratim Giri*², *Brian G. Trewyn*, *Michael P. Stellmaker*, *Victor S.-Y. Lin*³

Abstract

A superparamagnetic iron oxide nanoparticle-capped, MCM-41 type mesoporous silica nanorod-based controlled-release delivery system (Magnet-MSN) has been synthesized. We studied the stimuli-responsive release profiles of fluorescein-loaded Magnet-MSN delivery systems in the presence of external magnetic field by using cell-produced antioxidants as triggers for releasing fluorescein molecules. The intracellular delivery efficiency of the Magnet-MSN system with human cervical cancer cells (HeLa) *in vitro* was demonstrated.

Introduction

Recent reports on the synthesis of surface functionalized, superparamagnetic iron oxide nanoparticles for drug/gene delivery,¹⁻⁵ magnetic resonance imaging,⁶⁻⁹ bioseparation,¹⁰⁻¹³ tissue repairing,¹⁴ and thermal tumor therapy,¹⁵⁻¹⁸ have demonstrated the feasibility of using these magnetic nanoparticles for a variety of biological applications. In

¹ Reprinted with permission of Wiley-VCH Verlag GmbH & Co. KGaA

² Primary researcher and author

³ Author of correspondence

contrast, only a few magnetic nanoparticle-based controlled release drug delivery systems have been recently reported in the literature.^{19,20} Most of these systems consist of magnetic nanoparticle “cores” coated with organic or inorganic “shell” constituents. Pharmaceutical drugs are encapsulated inside the layers of shells. In the presence of an external magnetic field, these core-shell materials are attracted toward the magnet. This kind of magnetic motor effect is indeed attractive for future developments for site-specific drug delivery systems. However, many important site-selective deliveries, e.g., deliveries of highly toxic anti-tumor drugs require “zero release” before reaching the targeted cells or tissues. To the best of our knowledge, no magnetic nanoparticle-based controlled release delivery system that is stimuli-responsive and equipped with “zero premature release” capability has been reported previously.

In contrast, surface functionalized mesoporous silica materials have recently been demonstrated to be excellent carriers for hosting molecules of various sizes, shapes, and functionalities.²¹⁻²⁸ Particularly, recent reports²⁹⁻³³ on the design of capped and gated mesoporous silicas have offered promising potential for new generation of controlled release nanodevices. Herein, we report the synthesis of a superparamagnetic iron oxide nanoparticle-capped, MCM-41 type mesoporous silica nanorod-based controlled-released delivery system (Magnet-MSN) that is stimuli-responsive and chemically inert to the matrix-entrapped compounds. The system consists of a 3-(propylsulfanyl)propionic acid functionalized mesoporous silica nanorod (Linker-MSN) with an average particle size of 200 nm in length and 80 nm in width. The average pore diameter of the Linker-MSN is around 3.0 nm. As a proof of principle, fluorescein was used as the guest molecule to be encapsulated inside the Linker-MSN material. By introducing dry Linker-MSN particles to an aqueous solution of

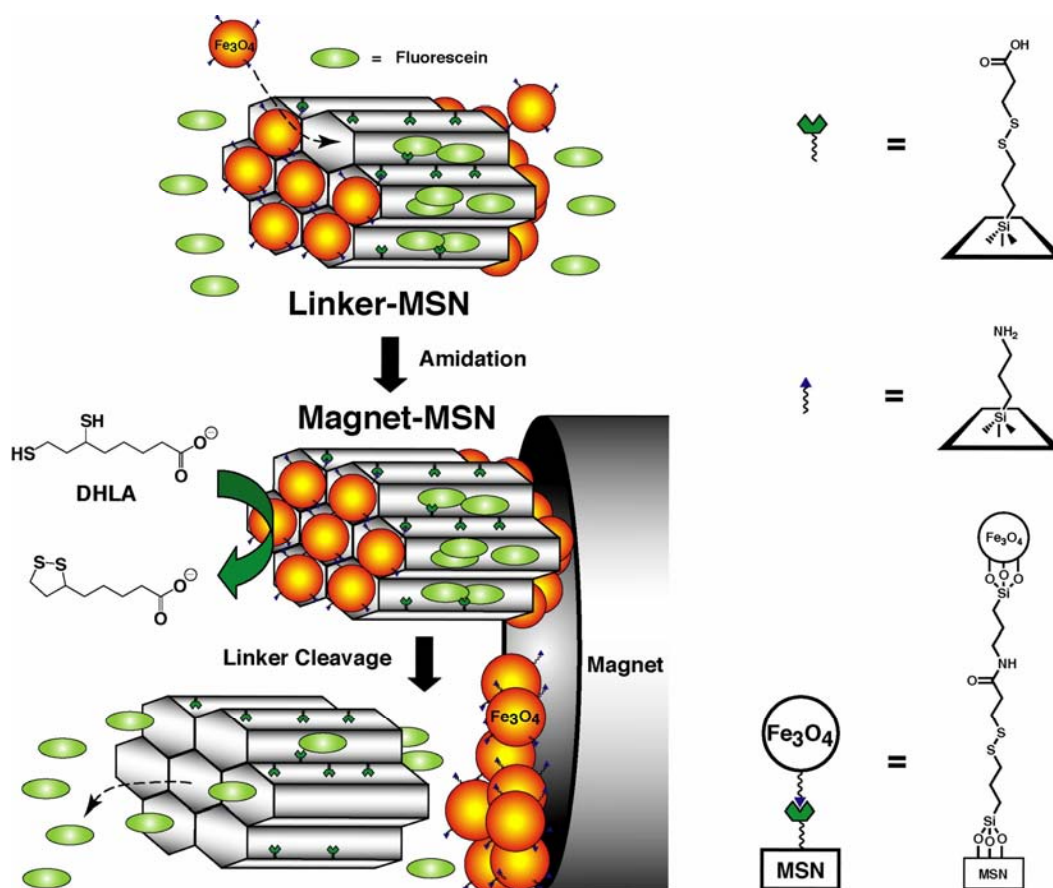


Figure 1. Schematic representation of the superparamagnetic iron oxide nanoparticle-capped mesoporous silica nanorod-based stimuli-responsive delivery system (Magnet-MSN). The controlled release mechanism of the system is based on chemical reduction of the disulfide linkage between the Fe_3O_4 nanoparticle caps and the Linker-MSN hosts by reducing agents, such as dihydrolipoic acid (DHLA).

fluorescein, the mesopores of the MSN could be used as reservoirs to soak up fluorescein molecules as depicted in Figure 1. Subsequently, the openings of the mesopores of the fluorescein-loaded Linker-MSN material were covalently capped *in situ*. This is facilitated by allowing the pore-surface bound 3-(propyldisulfanyl)propionic acid functional groups to covalently capture the 3-aminopropylsiloxy-derivatized, superparamagnetic iron oxide (APTS- Fe_3O_4) nanoparticles³⁴ via a literature-reported amidation reaction.³⁵ The resulting disulfide linkages between the MSNs and the Fe_3O_4 nanoparticles are chemically labile in

nature and can be cleaved with various cell-produced antioxidants and disulfide reducing agents, such as dihydrolipoic acid (DHLA) and dithiothreitol (DTT), respectively. Hence, the release of the magnetic nanoparticle caps from the fluorescein-loaded MSNs can be regulated by the concentration of trigger molecules (Figure 1).

Results and discussion

We first synthesized a rod-shaped mercaptopropyl-derivatized mesoporous silica nanomaterial (thiol-MSN) via our previously reported co-condensation method.^{31,33,36-38} The surfactant removed thiol-MSN material was treated with 2-carboxyethyl-2-pyridyl disulfide to yield the carboxy-functionalized Linker-MSN. The rod-like shape with an average particle size around 200 nm in length and 80 nm in width, and the MCM-41 type mesoporous structure are confirmed by transmission electron microscopy (TEM). The mesopores (porous channels) are represented by the alternating black and white stripes shown in Figure 2a. The N₂ sorption isotherms of the material further revealed a BET isotherm typical of MCM-41 structure (type IV) with a surface area of 1018.0 m²/g and a narrow BJH pore size distribution (average pore diameter = 3.0 nm).³⁹ The Linker-MSN (80.00 mg) was used as a chemically inert host to soak up the aqueous solutions of fluorescein (3.60 μM).

To design a chemically removable magnetic cap, we have synthesized a superparamagnetic Fe₃O₄ nanoparticle material coated with 3-aminopropylsiloxy groups (APTS-Fe₃O₄) via a literature-reported procedure.³⁴ The TEM micrograph (Figure 2b) of APTS-Fe₃O₄ showed an average particle size of 10 nm in diameter. As illustrated in Figure 1, the APTS-Fe₃O₄ nanoparticles (960.00 mg) were covalently captured and formed amide bonds by reacting with the mesopore surface-bound 3-(propyl-disulfanyl)propionic acid

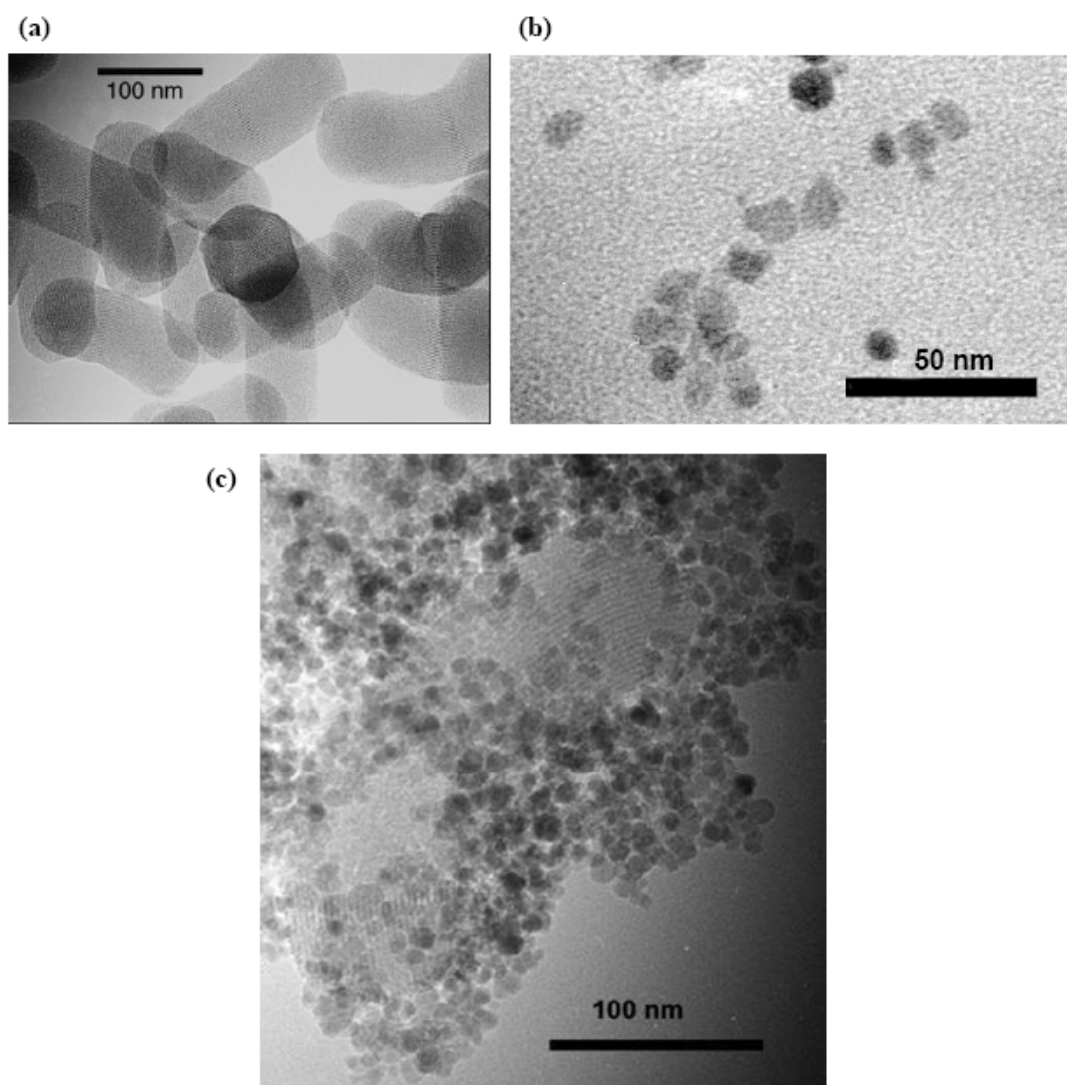


Figure 2. (a) Transmission electron micrographs (TEM) of Linker-MSN, (b) APTS-coated Fe₃O₄ nanoparticles, and (c) APTS-coated, Fe₃O₄ nanoparticle-capped Magnet-MSN.

groups of the Linker-MSN (80.00 mg) in a 3.60 μ M fluorescein solution in PBS (100.0 mM, pH 7.4). The resulting reaction suspensions were centrifuged and the Fe₃O₄-capped MSN/fluorescein material (Magnet-MSN) along with the unreacted APTS-Fe₃O₄ nanoparticles was filtered. The concentration of the free fluorescein molecules in the filtrate was then determined to be 1.50 μ M by UV-Vis absorption spectroscopy. The calculated

concentration decrease (ca. 2.10 μM) of fluorescein in solution was attributed to the amount of mesopore-encapsulated fluorescein (1.68×10^{-8} mol) per 80.00 mg of the Linker-MSN material. The number corresponds to ca. 58.3 mol% loading efficiency.

The successful incorporation of APTS- Fe_3O_4 nanoparticles to the MSN matrix was confirmed by various spectroscopic methods. As shown in Figure 3a, the covalent immobilization of the surface functionalized Fe_3O_4 nanoparticles to the Linker-MSN material reduced the intensity of the powder X-ray diffraction (XRD) peaks. Such a reduction of scattering contrast between the pores and the framework of the MCM-41 materials due to the pore-filling effect has been reported previously in the literature.⁴⁰⁻⁴³ Furthermore, a small increase in the d_{100} value of the Fe_3O_4 capped Magnet-MSN material in comparison with that of Linker-MSN was observed, which could also be attributed to the covalent linkage induced pore-filling effect between the Fe_3O_4 nanoparticles and the mesoporous silica matrix. The

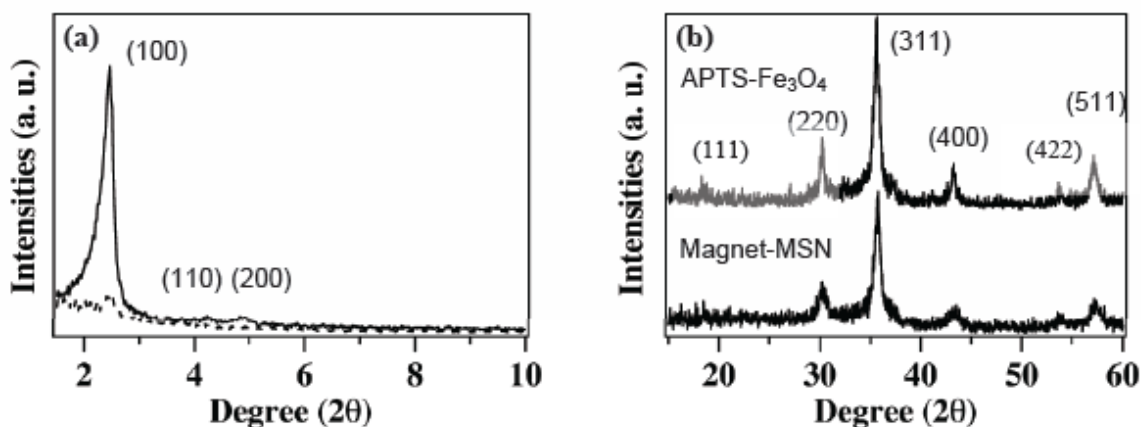


Figure 3. (a) Low angle powder X-ray diffraction (XRD) patterns of Linker-MSN (solid line) and Magnet-MSN (dashed line), (b) High angle XRD patterns of APTS-coated Fe_3O_4 nanoparticle (above) and Magnet-MSN (below).

high angle powder XRD patterns of the Magnet-MSN matched exactly with that of the synthesized APTS-Fe₃O₄ as shown in Figure 3b. This confirms the presence of APTS-Fe₃O₄ on the surface of Linker-MSN. The same pore-filling effect was also confirmed by the N₂ adsorption/desorption isotherms of the Fe₃O₄ capped Magnet-MSN materials. In contrast to the high surface area (1018.0 m²/g) of Linker-MSN, the Magnet-MSN showed a type I BET isotherm typical of non-porous materials with a surface area of 296.0 m²/g.³⁹ The results indicated that most of the pore openings of the Linker-MSN were indeed blocked by Fe₃O₄ nanoparticles. TEM investigations of the Magnet-MSN also provided direct evidence of the Fe₃O₄ nanoparticle distribution on the organically functionalized Linker-MSN material. As shown in Figure 2c, the Fe₃O₄ nanoparticles are clearly visible on the outside edge of the mesopores depicted by the dark particulate area. As opposed to these features observed in the case of Fe₃O₄-capped MSN, the TEM micrograph of the Linker-MSN (Figure 2a) prior to the Fe₃O₄ “capping” showed smooth edges and nice contrasts between the mesoporous channels and the silica matrix.

The disulfide linkages between the MSNs and Fe₃O₄ nanoparticles are chemically labile in nature and can be cleaved with disulfide-reducing agents to release the trapped guest molecules from the mesopores. As the entire Fe₃O₄-capped MSN carrier system is magnetic, the system can be magnetically directed to a site of interest from where the release can take place. In order to demonstrate the drug release under magnetic field, two cuvettes were charged with fluorescein loaded Magnet-MSN (50.0 mg each) dispersed in 3.00 mL of PBS buffer (100.0 mM, pH 7.4). Both cuvettes were held against the tips of two magnets (magnetic stir-bar retrievers). As illustrated in Figure 4a, all Magnet-MSNs were attracted to the walls of the cuvettes facing the tips of the external magnets. Dithiothreitol (DTT, 48.5

mg, 3.15×10^{-4} mol) was added to one of the two cuvettes (left) for the release experiment, while the other one (right) served as control. After two days (Figure 4b), green fluorescence was clearly observed in the solution in which DTT was added, whereas no fluorescence

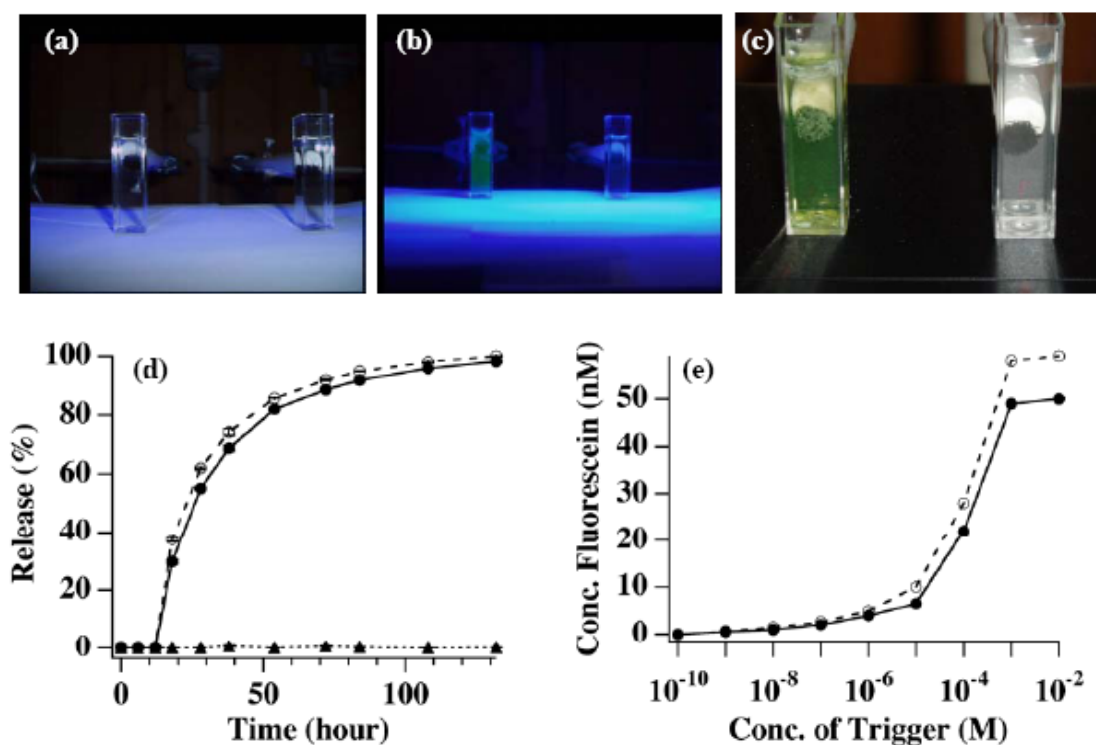


Figure 4. Photographs of two cuvettes charged with fluorescein loaded Magnet-MSN (50.0 mg each) dispersed in 3.00 mL of PBS buffer (100.0 mM, pH 7.4). **(a)** Accumulation of Magnet-MSNs on the walls of the cuvettes facing the tips of the external magnets (magnetic stir bar retrievers shown behind the cuvettes) was observed. **(b)** Green fluorescence was observed only in the solution in one of the two cuvettes (left) after 2 days of the addition of dithiothreitol (DTT, 48.5 mg). **(c)** The color of the accumulated Magnet-MSNs changed from black to gray after four days of DTT addition. **(d)** Controlled release of fluorescein from Magnet-MSN (13.0 mg) in 3.00 mL of 100.0 mM pH 7.4 PBS buffer over time triggered by 0.1 mM of dihydrolipoic acid (DHLA) (—●—) and DTT (--○--). No noticeable release was observed without the addition of trigger (···▲···). **(e)** The trigger concentration dependent releases. Released fluorescein concentrations were measured with Magnet-MSNs after 72 h of the additions of DHLA or DTT.

could be observed in the control solution. Given the fact the fluorescein loaded Magnet-MSN does not fluoresce due to the “fluorescence quenching” effect of Fe_3O_4 nanoparticle as described in recent literature reports,⁴⁴ the result indicated that fluorescein molecules were indeed released from the Magnet-MSNs by the introduction of disulfide reducing trigger, DTT. It is noteworthy that the color of the accumulated Magnet-MSNs near the external magnet changed from black to gray after four days of DTT addition as depicted Figure 4c. White precipitation of MSNs was also observed at the bottom of the cuvette. Given that the black Fe_3O_4 nanoparticles are attractive to the external magnetic field, whereas the MSNs are not, it is plausible that the free Fe_3O_4 nanoparticle caps were “pulled-in” toward the magnet, while the MSNs diffused away from the magnetic field as the disulfide linkage was cleaved by DTT.

As shown in Figure 4d, the Fe_3O_4 nanoparticle-capped MSN exhibited less than 1.0% of fluorescein release in 100.0 mM PBS buffer solutions (pH 7.4) over a period of 132 h without the introduction of trigger molecules. The result suggested a good capping efficiency of the Fe_3O_4 nanoparticles for encapsulation of fluorescein molecules against the undesired leaching problem. Addition of 0.1 mM of disulfide reducing molecules, such as DHLA and DTT, to a suspension of Magnet-MSNs (13.0 mg in 3.00 mL of 100.0 mM PBS pH 7.4 buffer) triggered a rapid release of the mesopore-entrapped fluorescein. Within 48 h, the release reached 85% of the total release of fluorescein, which took 5 days after the introduction of DHLA and DTT (Figure 4d). The maximum release of fluorescein is 40.0% and 31.4% of the total loading for DTT and reduced lipoic acid respectively. Interestingly, the rates of release of fluorescein by the two different triggers showed similar diffusional kinetic profiles indicating that the disulfide reducing abilities of DHLA and DTT are perhaps

comparable. This could be attributed to the fact that DHLA self-oxidizes into a disulfanyl-linked five-membered ring upon reducing the targeted disulfide bond, whereas DTT self-oxidized into a disulfanyl-linked six-membered ring. The thermodynamic incentives between cyclizations into five- and six-membered rings would be understandably similar. Furthermore, the amount of fluorescein release after 72 h of the addition of DHLA and DTT showed similar trigger concentration dependencies (Figure 4e) indicating that the rate of release was dictated by the rate of removing the Fe₃O₄ nanoparticle caps.

To investigate the endocytosis and biocompatibility of our system, Magnet-MSNs (0.2 mg/mL) were incubated with HeLa cells (~10⁵ cells/mL) overnight to allow the endocytosis of Magnet-MSNs.³³ The cells that contained Magnet-MSNs were magnetically separated from those without Magnet-MSNs. The isolated cells were treated with 0.001% of 4',6-diamidino-2-phenylindole (DAPI) dye in 100.0 mM PBS, pH 7.4 and placed in a cuvette. DAPI is known to form blue fluorescent complexes with natural double-stranded DNA and has been widely used as a fluorescent dye for nucleus staining. These DAPI-stained, fluorescent cells were first accumulated to the right side wall of the cuvette by applying an external magnetic field (a commercially available grade N45 neodymium iron boron magnet). When the magnet was moved to the left side of the cuvette, it could be clearly observed that the blue fluorescent HeLa cells moved across the cuvette toward the magnet as shown in Figure 5a-c. The result indicated that the Magnet-MSN could indeed be endocytosed by HeLa cells. To further confirm the endocytosis of Magnet-MSN, these HeLa cells were examined by fluorescence confocal microscopy. As displayed in the Supporting Information, a series of fluorescence images of different cross-sections of Magnet-MSN-containing HeLa cells were obtained by changing the focal depth every 1.2 μm vertically. As

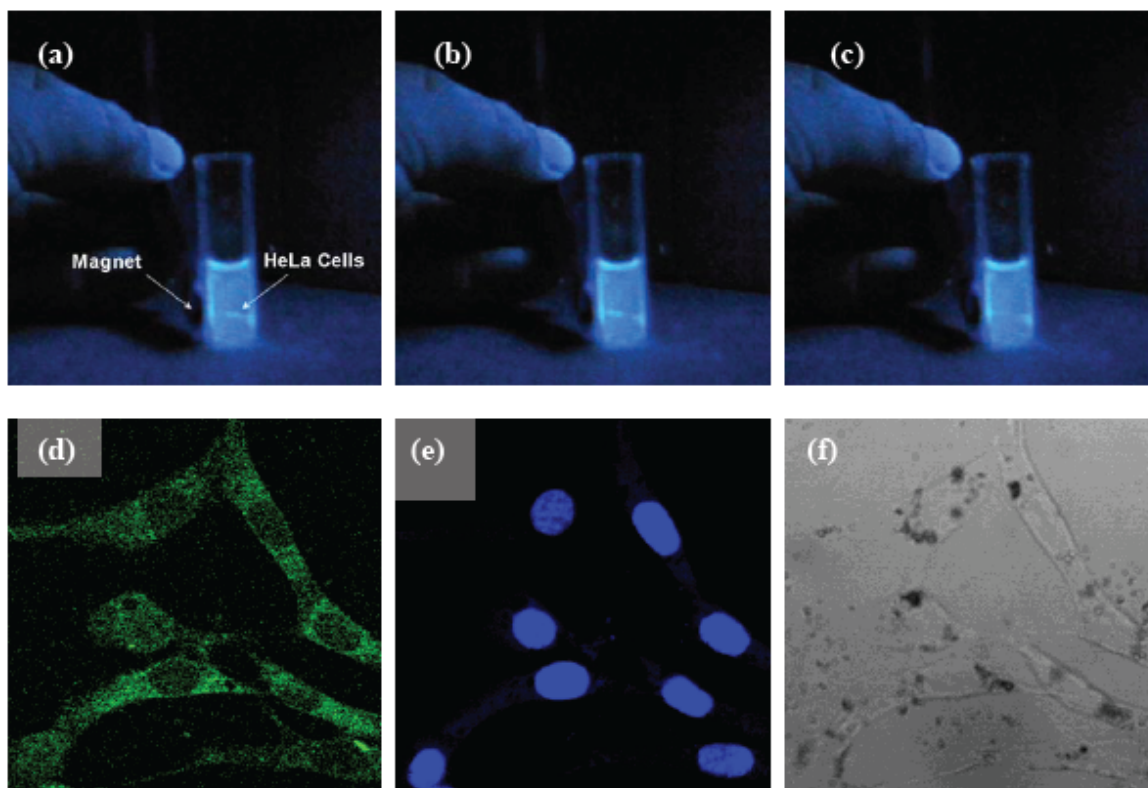


Figure 5. Panels (a), (b), and (c) are single frames of photographs of HeLa cells with Fe_3O_4 capped fluorescein loaded MSNs traveling across the cuvette, propelled by magnetic force. Panels (d), (e), and (f) are fluorescence confocal micrographs of HeLa cells after 10 h incubation with Fe_3O_4 capped fluorescein loaded MSNs. Micrograph (d) shows cells excited at 494 nm, whereas panel (e) are cells excited in the UV, and panel (f) is a pseudo-brightfield image, where dark aggregations of Magnet-MSNs could be clearly observed.

depicted in Figure 5d, green fluorescence could be clearly observed within the cell bodies of these HeLa cells upon excitation at 494 nm. The result strongly indicated that the mesopore-encapsulated fluorescein molecules were released inside of these cells. As previously reported by Biaglow and others, cancer cell-lines express significant amounts of DHLA.⁴⁵ We suspect that the efficient intracellular release of fluorescein was triggered by the high intracellular concentration of DHLA. To realize the locations of the nuclei, the cells were excited at 358 nm (Figure 5e). The appearance of healthy, intact nuclei in Figure 5e and

visibility of fully-grown cells by transmission in Figure 5f suggested that the Magnet-MSNs are biocompatible with HeLa cells *in vitro* under our experimental condition.

Conclusion

In conclusion, we have demonstrated that the superparamagnetic iron oxide nanoparticle-capped MSN material can be used as a novel controlled release delivery carrier that is stimuli responsive. Molecules that are smaller than 3 nm in size, such as fluorescein, could be encapsulated and released from the Magnet-MSN delivery system in the presence of external magnetic field by using cell-produced antioxidants (DHLA) as triggers. In addition, the good biocompatibility and intracellular delivery efficiency of the Magnet-MSN system with human cervical cancer cells offer promising potential in utilizing this system to investigate various inter- and intra-cellular chemical/neurochemical communications *in vitro*. We envision that this Magnet-MSN system could play a significant role in developing new generations of site-selective, controlled release delivery, and interactive sensory nanodevices.

Experimental section

$\text{FeCl}_2 \cdot 4\text{H}_2\text{O}$, $\text{FeCl}_3 \cdot 6\text{H}_2\text{O}$, 3-aminopropyltriethoxysilane (APTS), 3-mercaptopropionic acid, 2-aldrihiol, 3-mercaptopropyltrimethoxysilane (MPTMS), tetraethylorthosilicate (TEOS), *n*-cetyltrimethylammonium bromide (CTAB), 1-[3-(dimethylamino)propyl]-3-ethylcarbodiimide hydrochloride (EDC), fluorescein, and dithiothreitol (DTT) were purchased (Aldrich) and used as received. Reduced lipoic acid (DHLA) was obtained from Sigma and used without further purification. Nanopure water (18.1 MHz) prepared from a Barnstead E-pure water purification system was employed

throughout. PBS buffer (100.0 mM, pH 7.4) solutions were prepared and used as the solvent for all the loading experiments.

APTS coated magnetite (Fe_3O_4) nanoparticles: Synthesis and coating of magnetic nanoparticles were performed following a literature-reported procedure³⁴ with a slight modification (see supporting information in appendix).

MCM-41-type mesoporous silica nanoparticles with 3-(propyldisulfanyl)propionic acid functionality (Linker-MSN): The thiol-MSN material was synthesized via our previously published procedure³¹ with a slight modification (see supporting information in appendix). The purified thiol-MSN material (1.000 g) was treated with an ethanol solution (80.00 mL) of 2-carboxyethyl-2-pyridyl disulfide (1.340 g, 6.23×10^{-3} mol) which was synthesized via a literature procedure,⁴⁶ at room temperature for 24 h vigorous stirring to undergo the desired disulfide bond exchange reaction. The resulting MSN material with 3-(propyldisulfanyl)propionic acid functionality was filtered and washed with ethanol and dried in air. The chemically accessible thiol group surface coverage of the thiol-MSN material was quantified to be 7.01×10^{-4} mol/g by our previously published method.³⁸

Loading of fluorescein into the mesoporous framework of Linker-MSN and the capping of the mesopores with APTS coated Fe_3O_4 nanoparticles: The purified Linker-MSN material (80.0 mg) was stirred in an 8.00 mL PBS buffer solution (100.0 mM, pH 7.4) of fluorescein (3.6×10^{-6} M) for 24 h. The APTS coated Fe_3O_4 nanoparticles (960.0 mg) were added to the suspension, followed by the addition of 1-[3-(dimethylamino)propyl]-3-ethylcarbodiimide hydrochloride (EDC) (60.0 mg, 3.13×10^{-4} mol). The mixture was stirred for another 48h. The resulting precipitates were filtered, washed extensively with buffer and

finally dried under vacuum. The fluorescein loaded capped-MSN (480.0 mg) material was stirred again in 10.00 mL of PBS buffer (100.0 mM pH 7.4) for 48 h, followed by filtration and seven times washings to remove physisorbed, uncapped fluorescein molecules on the exterior surface of the material. The same material was suspended into 10.00 mL of PBS buffer (100.0 mM pH 7.4) for another 48 hour period, followed by filtration and seven times washings to further remove the physisorbed fluorescein and finally dried into powder. All the washings were collected. The loading of fluorescein (2.1×10^{-10} mol/mg of Linker-MSN) was calculated from the concentration difference between initial fluorescein solution and the resulting solution after the reaction and that of subsequent washings.

Endocytosis of Fe₃O₄ capped MSNs in HeLa cells: Human cervical cancer (HeLa) cell lines were obtained from American Tissue Culture Collection (ATCC). HeLa cells were maintained using DMEM (Dulbecco's modified Eagle's medium) supplemented with 10 % horse serum, 2.00 mM *L*-glutamine, 100 U/mL penicillin, 100.0 mg/mL streptomycin, and 1.0 mg/mL gentamicin.

HeLa cells were seeded onto 6-well plates (1×10^5 cells per well with 3.00 mL growth media) 24 h prior to the experiment. After 24 h the wells were seeded with 0.2 mg/mL Fe₃O₄ capped MSNs in growth media. After 10 h the media was removed and the cells were washed with new growth media. Following, the cells were trypsinized with 1× trypsin. A magnet was employed to keep the cells with nanorods stationary while all cells not affected by the magnet were removed. The remaining cells were centrifuged and resuspended in 100.0 mM PBS (pH 7.4) and 100.0 µg/mL DAPI.

References

- (1) Gupta, A. K.; Curtis, A. S. G. *Journal of Materials Science: Materials in Medicine* **2004**, *15*, 493-496.
- (2) Neuberger, T.; Schoepf, B.; Hofmann, H.; Hofmann, M.; von Rechenberg, B. *Journal of Magnetism and Magnetic Materials* **2005**, *293*, 483-496.
- (3) Lubbe, A. S.; Bergemann, C.; Brock, J.; McClure, D. G. *Journal of Magnetism and Magnetic Materials* **1999**, *194*, 149-155.
- (4) Schillinger, U.; Brill, T.; Rudolph, C.; Huth, S.; Gersting, S.; Kroetz, F.; Hirschberger, J.; Bergemann, C.; Plank, C. *Journal of Magnetism and Magnetic Materials* **2005**, *293*, 501-508.
- (5) Scherer, F.; Anton, M.; Schillinger, U.; Henke, J.; Bergemann, C.; Kruger, A.; Gansbacher, B.; Plank, C. *Gene Therapy* **2002**, *9*, 102-109.
- (6) Perez, J. M.; Josephson, L.; O'Loughlin, T.; Hoegemann, D.; Weissleder, R. *Nature Biotechnology* **2002**, *20*, 816-820.
- (7) Perez, J. M.; O'Loughlin, T.; Simeone, F. J.; Weissleder, R.; Josephson, L. *Journal of the American Chemical Society* **2002**, *124*, 2856-2857.
- (8) Bulte, J. W. M.; Douglas, T.; Witwer, B.; Zhang, S.-C.; Strable, E.; Lewis, B. K.; Zywicke, H.; Miller, B.; van Gelderen, P.; Moskowitz, B. M.; Duncan, L. D.; Frank, J. A. *Nature Biotechnology* **2001**, *19*, 1141-1147.
- (9) Gellissen, J.; Axmann, C.; Prescher, A.; Bohndorf, K.; Lodemann, K. P. *Magnetic Resonance Imaging* **1999**, *17*, 557-567.
- (10) Doyle, P. S.; Bibette, J.; Bancaud, A.; Viovy, J.-L. *Science (Washington, DC, United States)* **2002**, *295*, 2237.

- (11) Wang, D.; He, J.; Rosenzweig, N.; Rosenzweig, Z. *Nano Letters* **2004**, *4*, 409-413.
- (12) Xu, C.; Xu, K.; Gu, H.; Zheng, R.; Liu, H.; Zhang, X.; Guo, Z.; Xu, B. *Journal of the American Chemical Society* **2004**, *126*, 9938-9939.
- (13) Gu, H.; Ho, P.-L.; Tsang, K. W. T.; Wang, L.; Xu, B. *Journal of the American Chemical Society* **2003**, *125*, 15702-15703.
- (14) Gupta, A. K.; Gupta, M. *Biomaterials* **2005**, *26*, 3995-4021.
- (15) Jordan, A.; Scholz, R.; Wust, P.; Schirra, H.; Schiestel, T.; Schmidt, H.; Felix, R. *Journal of Magnetism and Magnetic Materials* **1999**, *194*, 185-196.
- (16) Hilger, I.; Andra, W.; Hergt, R.; Hiergeist, R.; Schubert, H.; Kaiser, W. A. *Radiology* **2001**, *218*, 570-5.
- (17) Chan, D. C. F.; Kirpotin, D. B.; Bunn, a. P. A., Jr. *Journal of Magnetism and Magnetic Materials* **1993**, *122*, 374-8.
- (18) Hirsch, L. R.; Stafford, R. J.; Bankson, J. A.; Sershen, S. R.; Rivera, B.; Price, R. E.; Hazle, J. D.; Halas, N. J.; West, J. L. *Proceedings of the National Academy of Sciences of the United States of America* **2003**, *100*, 13549-13554.
- (19) Yoon, T.-J.; Kim, J. S.; Kim, B. G.; Yu, K. N.; Cho, M.-H.; Lee, J.-K. *Angewandte Chemie, International Edition* **2005**, *44*, 1068-1071.
- (20) Chattopadhyay, P.; Gupta, R. B. *Industrial & Engineering Chemistry Research* **2002**, *41*, 6049-6058.
- (21) Diaz, J. F.; Balkus, K. J., Jr. *J. Mol. Catal. B: Enzymatic* **1996**, *2*, 115-126.
- (22) Han, Y.-J.; Stucky, G. D.; Butler, A. J. *Am. Chem. Soc.* **1999**, *121*, 9897-9898.
- (23) Takahashi, H.; Li, B.; Sasaki, T.; Miyazaki, C.; Kajino, T.; Inagaki, S. *Microporous Mesoporous Mater.* **2001**, *44-45*, 755-762.

- (24) Vallet-Regi, M.; Ramila, A.; del Real, R. P.; Perez-Pariente, J. *Chem. Mater.* **2001**, *13*, 308-311.
- (25) Munoz, B.; Ramila, A.; Perez-Pariente, J.; Diaz, I.; Vallet-Regi, M. *Chem. Mater.* **2003**, *15*, 500-503.
- (26) Ramila, A.; Munoz, B.; Perez-Pariente, J.; Vallet-Regi, M. *J. Sol.-Gel Sci. Technol.* **2003**, *26*, 1199-1202.
- (27) Tourne-Peteilh, C.; Brunel, D.; Begu, S.; Chiche, B.; Fajula, F.; Lerner, D. A.; Devoisselle, J.-M. *New J. Chem.* **2003**, *27*, 1415-1418.
- (28) Vallet-Regi, M.; Doadrio, J. C.; Doadrio, A. L.; Izquierdo-Barba, I.; Perez-Pariente, J. *Solid State Ionics* **2004**, *172*, 435-439.
- (29) Mal, N. K.; Fujiwara, M.; Tanaka, Y. *Nature (London)* **2003**, *421*, 350-353.
- (30) Hernandez, R.; Tseng, H.-R.; Wong, J. W.; Stoddart, J. F.; Zink, J. I. *J. Am. Chem. Soc.* **2004**, *126*, 3370-3371.
- (31) Lai, C.-Y.; Trewyn, B. G.; Jeftinija, D. M.; Jeftinija, K.; Xu, S.; Jeftinija, S.; Lin, V. S. Y. *Journal of the American Chemical Society* **2003**, *125*, 4451-4459.
- (32) Gruenhagen, J. A.; Lai, C.-Y.; Radu, D. R.; Lin, V. S. Y.; Yeung, E. S. *Appl. Spectrosc.* **2005**, *59*, 424-431.
- (33) Radu, D. R.; Lai, C.-Y.; Jeftinija, K.; Rowe, E. W.; Jeftinija, S.; Lin, V. S. Y. *Journal of the American Chemical Society* **2004**, *126*, 13216-13217.
- (34) Ma, M.; Zhang, Y.; Yu, W.; Shen, H.-y.; Zhang, H.-q.; Gu, N. *Colloids and Surfaces, A: Physicochemical and Engineering Aspects* **2003**, *212*, 219-226.
- (35) Chan, W. C. W.; Nie, S. *Science (Washington, D. C.)* **1998**, *281*, 2016-2018.

- (36) Huh, S.; Wiench Jerzy, W.; Trewyn, B. G.; Song, S.; Pruski, M.; Lin, V. S. Y. *Chem. Commun.* **2003**, 2364-5.
- (37) Huh, S.; Wiench, J. W.; Yoo, J.-C.; Pruski, M.; Lin, V. S. Y. *Chem. Mater.* **2003**, *15*, 4247-4256.
- (38) Lin, V. S. Y.; Lai, C.-Y.; Huang, J.; Song, S.-A.; Xu, S. *Journal of the American Chemical Society* **2001**, *123*, 11510-11511.
- (39) See supporting information in appendix for details.
- (40) Marler, B.; Oberhagemann, U.; Vortmann, S.; Gies, H. *Microporous Materials* **1996**, *6*, 375-383.
- (41) Winkler, H.; Birkner, A.; Hagen, V.; Wolf, I.; Schmechel, R.; Von Seggern, H.; Fischer, R. A. *Advanced Materials (Weinheim, Germany)* **1999**, *11*, 1444-1448.
- (42) Zhang, W.-H.; Shi, J.-L.; Wang, L.-Z.; Yan, D.-S. *Chemistry of Materials* **2000**, *12*, 1408-1413.
- (43) Zhang, W.-H.; Shi, J.-L.; Chen, H.-R.; Hua, Z.-L.; Yan, D.-S. *Chemistry of Materials* **2001**, *13*, 648-654.
- (44) Josephson, L.; Kircher, M. F.; Mahmood, U.; Tang, Y.; Weissleder, R. *Bioconjugate Chemistry* **2002**, *13*, 554-560.
- (45) Biaglow, J. E.; Donahue, J.; Tuttle, S.; Held, K.; Chrestensen, C.; Mieyal, J. *Analytical Biochemistry* **2000**, *281*, 77-86.
- (46) Carlsson, J.; Drevin, H.; Axen, R. *Biochemical Journal* **1978**, *173*, 723-37.

Appendix

Supporting information

Instrumental methods, conditions, and parameters for the structure characterizations of Linker-MSN and Fe₃O₄-capped MSN materials: Powder XRD diffraction data were collected on a Scintag XRD 2000 X-ray diffractometer using Cu K α radiation. Nitrogen adsorption and desorption isotherm, surface area (SA), and median pore diameter (MPD) were measured using a Micromeritics ASAP2000 sorptometer. Sample preparation included degassing at 90 °C for 1 h. Nitrogen adsorption and desorption isotherms of these materials were obtained at -196 °C. Specific surface areas and pore size distributions were calculated using the Brunauer-Emmett-Teller (BET) and Barrett-Joyner-Halenda (BJH) method, respectively. Particle morphology of these materials was determined by scanning electron microscopy (SEM) using a JEOL 840A scanning electron microscope with 10 kV accelerating voltage and 0.005 nA of beam current for imaging. For transmission electron microscopy measurements, a small aliquot was ground with methanol in an agate mortar and pestle. A single drop of this suspension was placed on a lacey carbon coated copper TEM grid and dried in air. The TEM examination was completed on a Philips model CM-30 operated at 300 kV at 69,000 to 340,000 electron optical magnification. Study of fluorescein release kinetics and different concentrations of fluorescein released under the varying dosage concentration of reduced lipoic acid and DTT were done by recording the fluorescence emission spectra of the aliquots using fluorometer (Fluoromax-2[®]) and matching the fluorescence intensities with that of the calibrated standard results.

APTS Coated Magnetite (Fe₃O₄) Nanoparticles: Ammonium hydroxide (1.50 M) was added drop wise into a vigorously stirred deoxygenated aqueous solution (600.0 mL, pH 1.5) of iron(II) chloride tetrahydrate (498.0 mg, 2.50×10^{-3} mol) and iron(III) chloride hexahydrate (810.0 mg, 2.99×10^{-3} mol). Addition of ammonium hydroxide was continued till the pH of the solution reached 9.0 from 1.5 and black precipitate of magnetite (Fe₃O₄) formed immediately. The black precipitate was separated by magnetic decantation, washed five times with water, two times with ethanol and finally evaporated to dryness to get Fe₃O₄ powder. The obtained magnetite powder (298.0 mg) was then sonicated in 600.0 mL of

ethanol with 4.00 mL of H₂O. To this suspension, 3-aminopropyl triethoxysilane (APTS, 113.0 mg, 5.11×10^{-4} mol) was added and was stirred overnight yielding APTS coated magnetite nanoparticles in the form of a brown powder which was isolated after filtering and vacuum drying the reaction mixture.

MCM-41-type mesoporous silica nanorods (thiol-MSN): The thiol-MSN material was synthesized by the following procedure: *n*-Cetyltrimethylammonium bromide (CTAB, 1.00 g, 2.74×10^{-3} mol) was first dissolved in 480 mL of Nanopure water. NaOH(aq) (2.00 M, 3.50 mL) was added to CTAB solution, followed by adjusting the solution temperature to 353 K. TEOS (5.00 mL, 2.57×10^{-2} mol) and MPTMS (0.5 mL, 2.64×10^{-3} mol) was added to the solution simultaneously drop wise for a period of 4 min. The mixture was allowed to stir for 2 h to give rise to white precipitates (as synthesized thiol-rods). The solid product was filtered, washed with deionized water and methanol, and dried in air. To remove the surfactant template (CTAB), 1.50 g of as synthesized thiol-rod was refluxed for 24 h in a solution of 6 mL of HCl (37.4%) and 160 mL of methanol followed by extensive washes with deionized water and methanol. The resulting surfactant removed thiol-MSN material was placed under high vacuum to remove the remaining solvent in the mesopores.

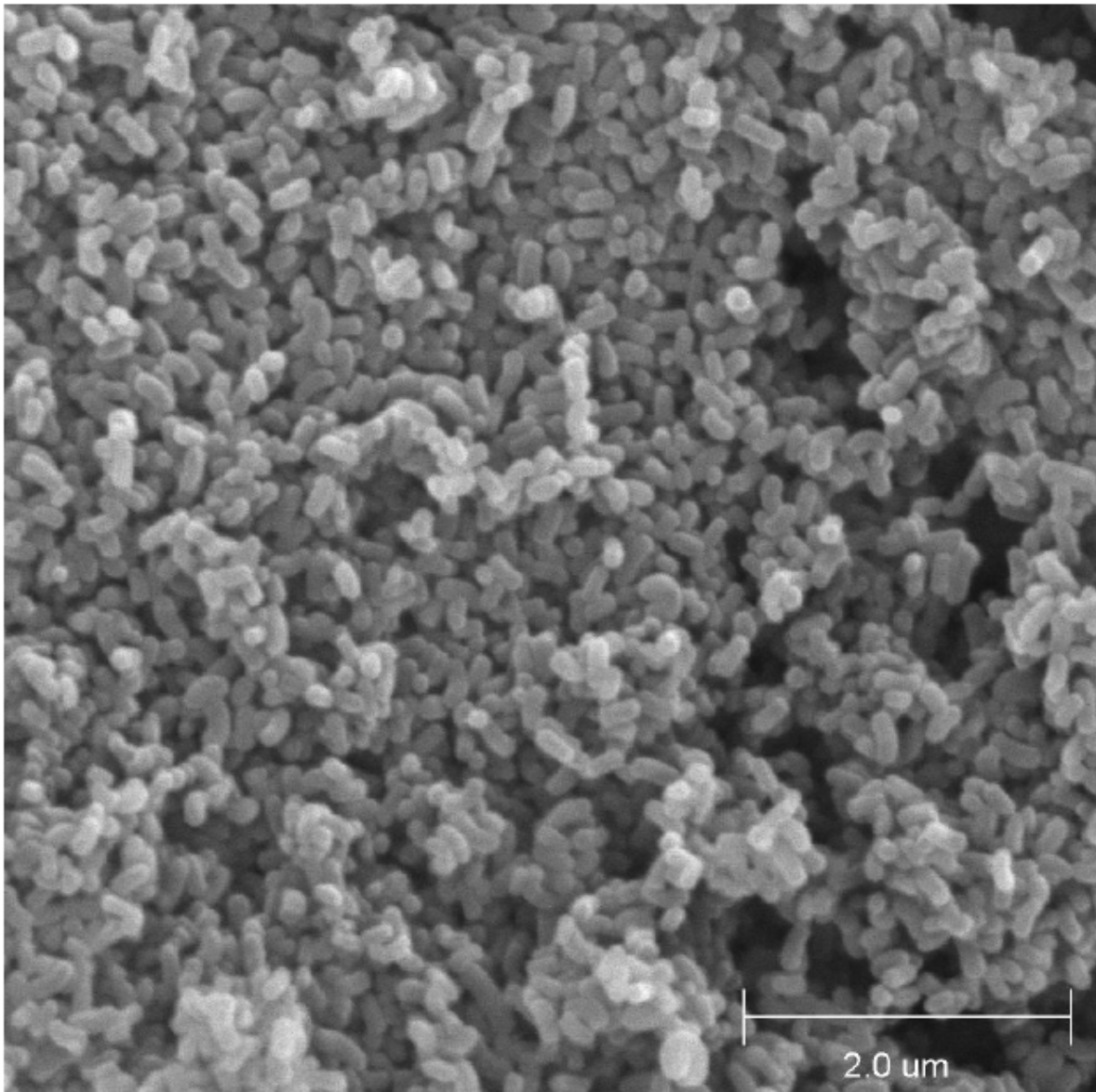


Figure S1. Scanning electron micrograph (SEM) of the rod-like Linker-MSN.

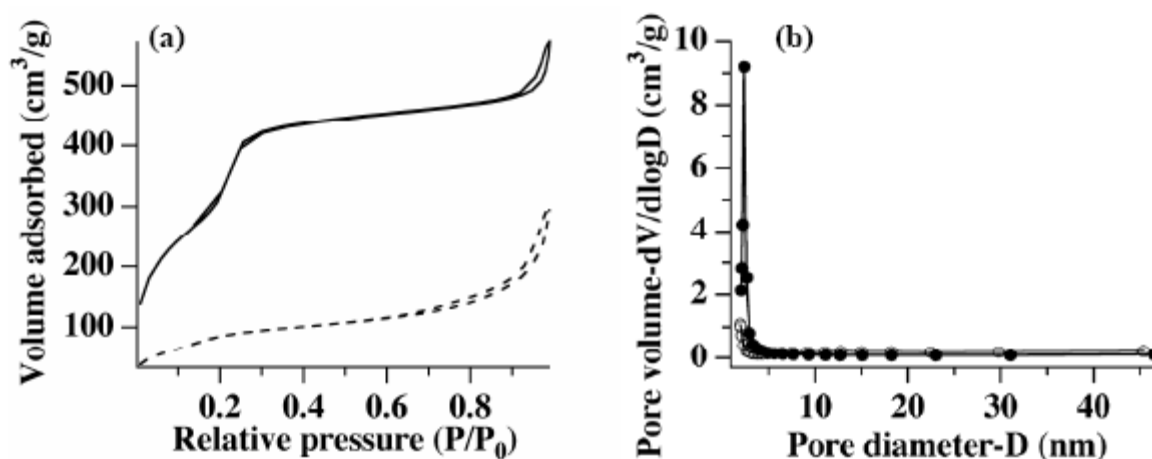


Figure S2. (a) BET nitrogen sorption isotherms of the Linker-MSN (solid line) and Magnet-MSN (dashed line) materials. (b) BJH pore size distributions for the Linker-MSN (—○—) and Magnet-MSN (—λ—) materials. The decrease in surface area and the disappearance of the maximum peak in BJH pore size distribution plot indicate that the mesopores of MSN are capped by the APTS coated Fe₃O₄ nanoparticles.

Table S1. Structural parameters of the Linker-MSN and the Magnet-MSN materials

Material	BET surface area (m ² /g)	BET pore volume (mL/g)	BJH pore diameter (Å)
Linker-MSN	1018	0.79	30.0
Magnet-MSN	296	0.36	--

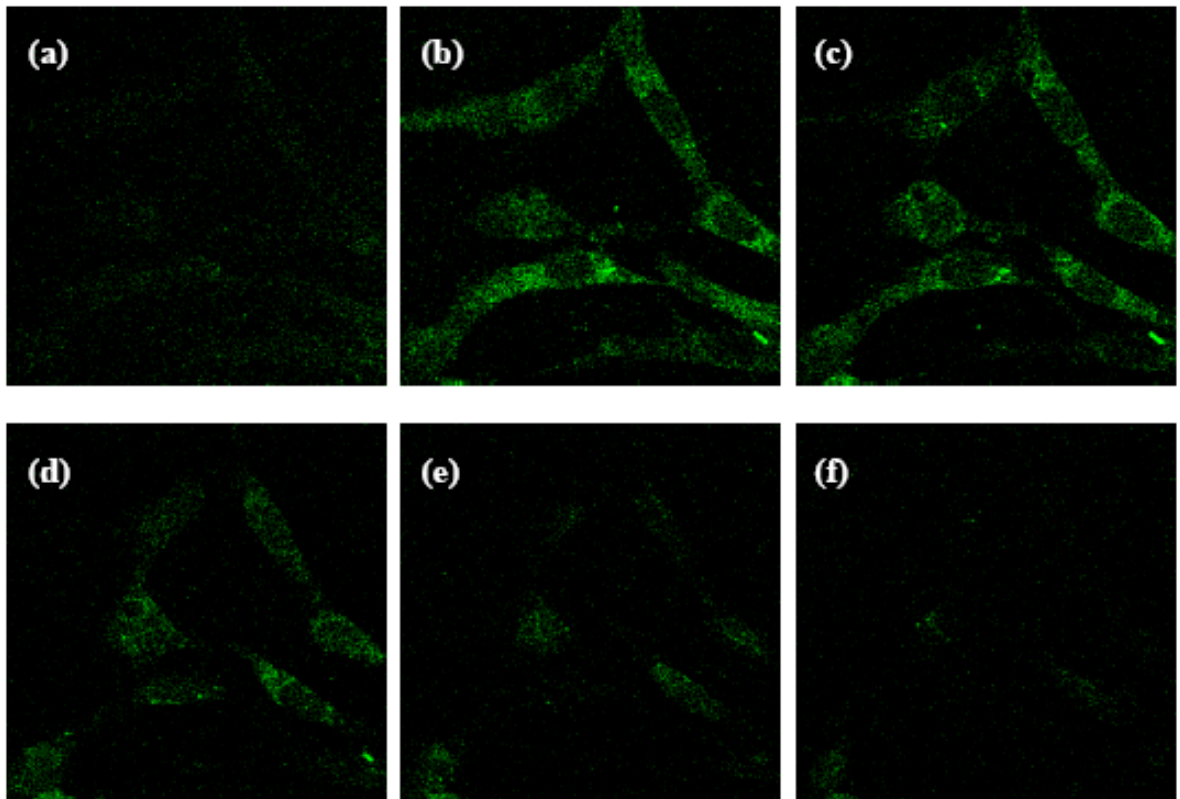


Figure S3. Fluorescence confocal micrographs of HeLa cells after 10 h incubation demonstrating endocytosis of Magnet-MSNs (a)-(f). Each frame represents a focal point with 1.2 μm vertical difference.

CHAPTER 3. INHIBITION OF GROWTH OF HUMAN CERVICAL CANCER CELL LINE (HeLa) BY INTRACELLULAR RELEASE OF A DNA-INTERCALATING DRUG FROM MAGNETIC NANOPARTICLE CAPPED MESOPOROUS SILICA NANORODS

Supratim Giri, Igor I. Slowing, Victor S. -Y. Lin

Abstract

A successful *in vitro* experiment demonstrating the loading and release of a DNA intercalating drug 9-aminoacridine was performed using magnetic nanoparticle capped mesoporous silica nanorods (Magnet-MSN) by the action of reductant triggers. The *in vivo* application of Magnet-MSN with HeLa cells led to the enhanced cell growth inhibition effect. The cell growth inhibition was found to be unaffected by a strong external magnetic field.

Introduction

A major focus of biological application that involves nanostructured materials had been shifted towards the progress of cancer chemotherapy in recent times.¹ Development of targeted as well as stimuli responsive delivery systems of therapeutic agents has occupied utmost interest in that context as the idea of delivering drug molecules to the target without damaging the healthy tissue has made the approach of chemotherapy more attractive.² The nanoscale materials that are being utilized for drug delivery include liposomes,³ polymer/drug conjugates,⁴ polymer-DNA complexes⁵ and polymeric micelles^{6,7} etc. However, polymer and liposome based drug delivery agents suffer from several drawbacks

such as the complexity that arises from the modification of drug molecules to incorporate them inside the polymeric or liposomal vesicles. Sometimes additional functionalization of those vesicles are required for the recognition by a specific cell type and the vesicles sometime break down as soon as those enter inside the cell and therefore no controlled release property is observed. In contrast, the magnetic nanoparticle capped mesoporous silica nanorods that were developed in our group displays excellent *in vivo* stimuli responsive controlled release properties, biocompatibility and are very stable against any type of enzymatic biodegradation.⁸ Furthermore, the magnetic property of the above delivery system can be utilized as a targeting tool towards a particular cell type or tissue of interest.

In this chapter, we report the intracellular delivery of a DNA intercalating mutagen 9-aminoacridine (abbreviated as 9AA)⁹⁻¹¹ which was loaded inside functionalized mesoporous silica nanorods (MSN) capped with magnetic nanoparticles. In our previous studies, we successfully demonstrated the encapsulation and stimuli responsive controlled release of fluorescein molecules entrapped inside the organo-functionalized MSNs capped with surface functionalized magnetic nanoparticles.⁸ In the present study, the mutagenic drug 9AA was loaded inside a similar system, which consists of MSNs functionalized with 3-(propylsulfanyl)propionic acid, termed as “Linker-MSNs”. These dry Linker-MSNs were soaked in the aqueous solution of 9-aminoacridine to incorporate the mutagen molecules inside the mesoporous channels of the host material. Next, the openings of the mesopores of the 9AA-loaded Linker-MSNs were covalently capped in situ through the amidation of the carboxylic acid functional groups bound at the pore surface with amine functionalized superparamagnetic iron oxide (APTS-Fe₃O₄) nanoparticles. The magnetic nanoparticle capped 9AA containing MSNs were termed as “Magnet-MSNs”. The chemically labile

nature of the disulfide linkages between the MSNs and the inorganic nanoparticles have already been demonstrated with various cell-produced antioxidants and disulfide reducing agents such as dihydrolipoic acid (DHLA) and dithiothreitol (DTT), respectively.⁸ As a result of the incubation of 9AA loaded Magnet-MSNs with HeLa cells, an inhibition effect of the growth of HeLa cell lines were observed upon the internalization of the material.

Results and discussions

The rod shaped (200 nm × 80 nm) Linker-MSNs were prepared from surfactant washed mercaptopropyl-derivatized mesoporous silica (thiol-MSNs) following our previously published literature methods.⁸ These Linker-MSNs are of MCM-41 type with very high surface area (1081 m²g⁻¹) and narrow pore size distribution (average pore diameter: 3.0 nm).⁸ The superparamagnetic Fe₃O₄ nanoparticles having an average diameter of 10 nm coated with 3-aminopropylsiloxy groups (APTS-Fe₃O₄) were also prepared according to our previously published literature.⁸ In the presence of an aqueous solution of 9AA (1.13×10⁻⁴ M) in PBS medium (10.0 mM, pH 7.4), Linker-MSNs were treated with APTS-Fe₃O₄ by a coupling agent (EDC). The loading of 9AA was found out to be 5.3 × 10⁻⁶ mol per g of Linker-MSN by subtracting the concentration of the unloaded 9AA (0.9×10⁻⁴ M) from the initial concentration of standard solution of 9AA (1.13×10⁻⁴ M). The loading was calculated to be 20.0 mole% in terms of loading efficiency.

In order to study the release kinetics of the mutagen 9AA from the Magnet-MSNs by disulfide reducing triggers, several *in vitro* experiments were done. In a typical experiment, Magnet-MSNs (13.0 mg) were accumulated on the inner surface of a vertical wall of a cuvette by a small piece of magnet. Under controlled condition, where no reducing agents

were present, almost no release (less than 1%) of 9AA from the Magnet-MSNs in PBS (3.0 mL, pH 7.4, 10 mM) was observed over a period of 72 h (Figure 1a). This observation demonstrated the zero release property of Magnet-MSNs in the absence of chemical stimuli. Upon introduction of the disulfide reducing agent dihydrolipoic acid (DHLA, 1.13×10^{-4} M solution in PBS), release of 9AA was observed and the release kinetics were recorded (Figure 1a).

The normalized release plot revealed the typical diffusion based release kinetics of 9AA from the mesopores of Linker-MSN. A stronger reducing agent DTT (1.13×10^{-4} M solution in PBS) induced a relatively faster release of 9AA following the same diffusion pattern. In order to demonstrate the stimuli responsive property of 9AA loaded Magnet-MSNs, different concentrations of the reducing trigger DHLA as well as DTT were also

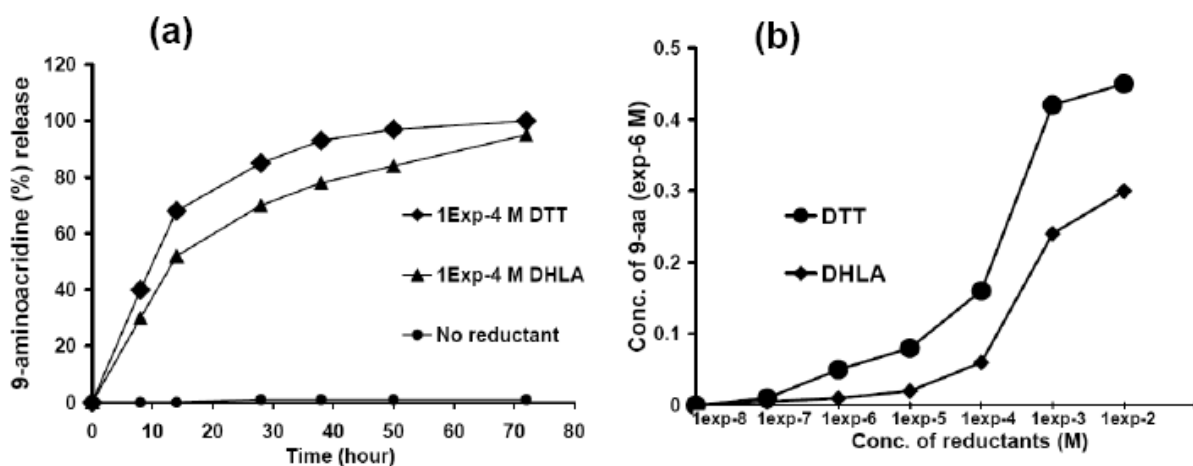


Figure 1. Study of the kinetics of release of 9AA from Magnet-MSNs by disulfide reductant triggers: (a) controlled release of 9AA from Magnet-MSN (13.0 mg) dispersed in 3.00 mL of PBS solution (pH7.4, 10 mM) triggered by 1.0×10^{-4} M DTT or DHLA; no noticeable release was observed in the absence of reductant. (b) The dependence of the release of 9AA from Magnet-MSN (13.0 mg) dispersed in 3.00 mL of PBS solution (pH7.4, 10 mM) on the concentration of the reductant, measured 48 h after the addition of DTT or DHLA.

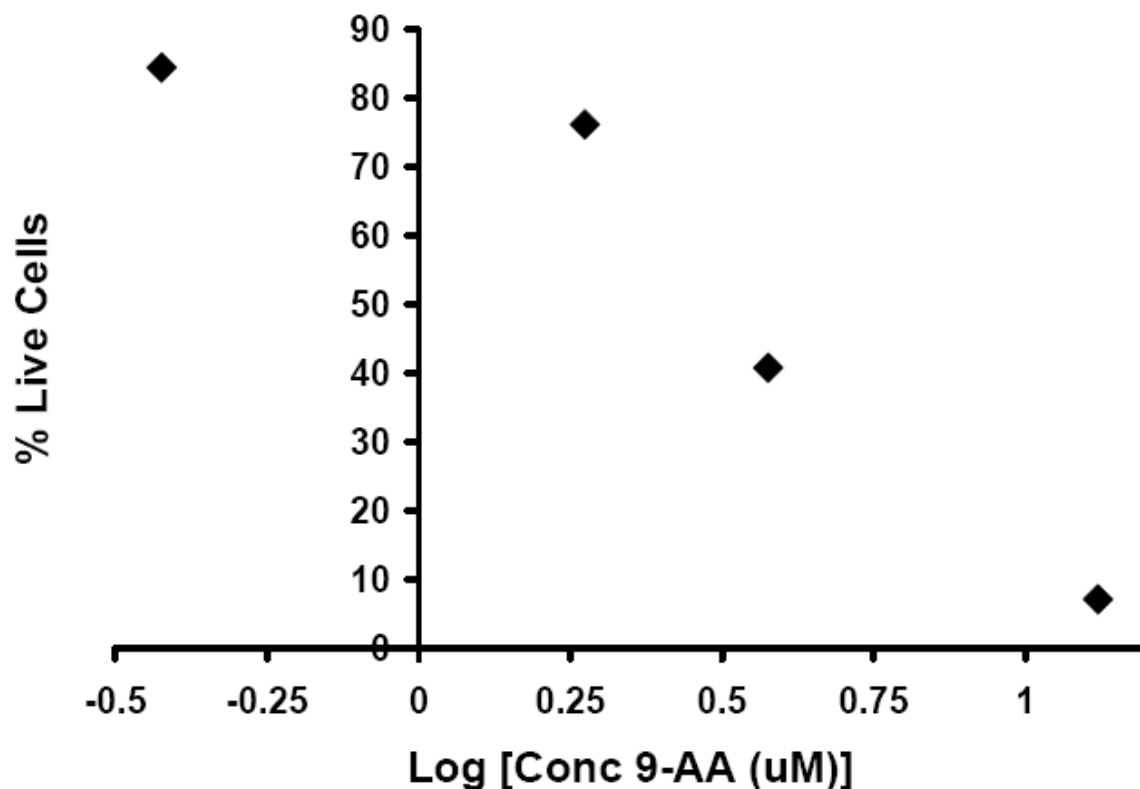


Figure 2. Plot for determination of LD₅₀ value for the drug 9AA in PBS (pH 7.4, 10 mM) with respect to HeLa cells. The percentage of live cells are plotted against the 9AA dosage concentration and the results that are obtained after 2 days of incubation are shown here.

applied to observe the concentration dependent release of the mutagen molecules from Magnet-MSNs (Figure 1b). This observation supported the logic that the rate of release of 9AA was dictated by the rate at which the disulfide linkage between Linker-MSNs and Fe₃O₄ nanoparticles were reduced.

In order to measure the cytotoxicity of the mutagen 9AA, HeLa cells were incubated with various concentration of 9AA in growth media and the corresponding cell viability was measured. The concentration of 9AA at which about 50% of cells were dead (LC₅₀) was found out to be 3.0×10^{-6} M (Figure 2). To demonstrate the drug delivery efficacy of 9AA-

Magnet-MSNs and to figure out whether the intracellular release of drugs is affected by magnetic field at all, we performed a series of three different cell culture experiments. As a control, we synthesized empty Magnet-MSNs where there is no drug loaded inside the MSNs but magnetic nanoparticle caps are linked with Linker-MSN via disulfide linkage. The typical half maximal effective concentration (EC_{50}) value of Magnet-MSNs was found to be in the range of $50.0 \mu\text{g mL}^{-1}$. HeLa cells were separately incubated with empty Magnet-MSNs ($50.0 \mu\text{g mL}^{-1}$) as well as 9AA loaded Magnet-MSNs ($50.0 \mu\text{g mL}^{-1}$), respectively. After 2 days of incubation, the percentage of live cells were calculated and compared with the normal growth of HeLa cells that do not have any Magnet-MSNs as a control (Figure 3). Interestingly, the cells that were incubated with 9AA loaded Magnet-MSNs showed almost 45% decrease in cell growth compared to the untreated (no Magnet MSNs) growth of HeLa cells, whereas the cells that were incubated with empty Magnet-MSNs exhibited only 10% decrease in cell growth. This important observation suggests that empty Magnet-MSNs are still biocompatible with HeLa cells, as in the absence of 9AA no considerable decrease of cell growth was observed. The cells that were incubated with 9AA loaded magnet-MSNs showed a significant cell growth inhibition. We believe that Magnet-MSNs were internalized by the HeLa cells in each of the above cases, as we have already seen the endocytosis of fluorescein loaded Magnet-MSNs when incubated with the same cell line in growth media.⁸ As the human cervical cancer cell lines HeLa are known to over express cell produced antioxidant DHLA,¹² introduction of 9AA loaded Magnet-MSNs into the HeLa cells led to the intracellular reduction of the disulfide linkage between the Linker-MSN and the magnetic nanoparticles and the subsequent drug release induced the cell enhanced cell death. The striking feature of the above experiment lies in the fact of drug delivery efficacy. It may be

noted that the concentration corresponding to the LC_{50} value of 9AA in PBS is 3.0×10^{-6} M, whereas the total concentration of 9AA that is present in $50 \mu\text{g Magnet-MSN mL}^{-1}$ of the cell culture media corresponds to 4.0×10^{-8} M. So using the Magnet-MSN system, it is possible to deliver drugs effectively inside the HeLa cells at a concentration which is less than two orders of magnitude of the LC_{50} concentration of the corresponding drug.

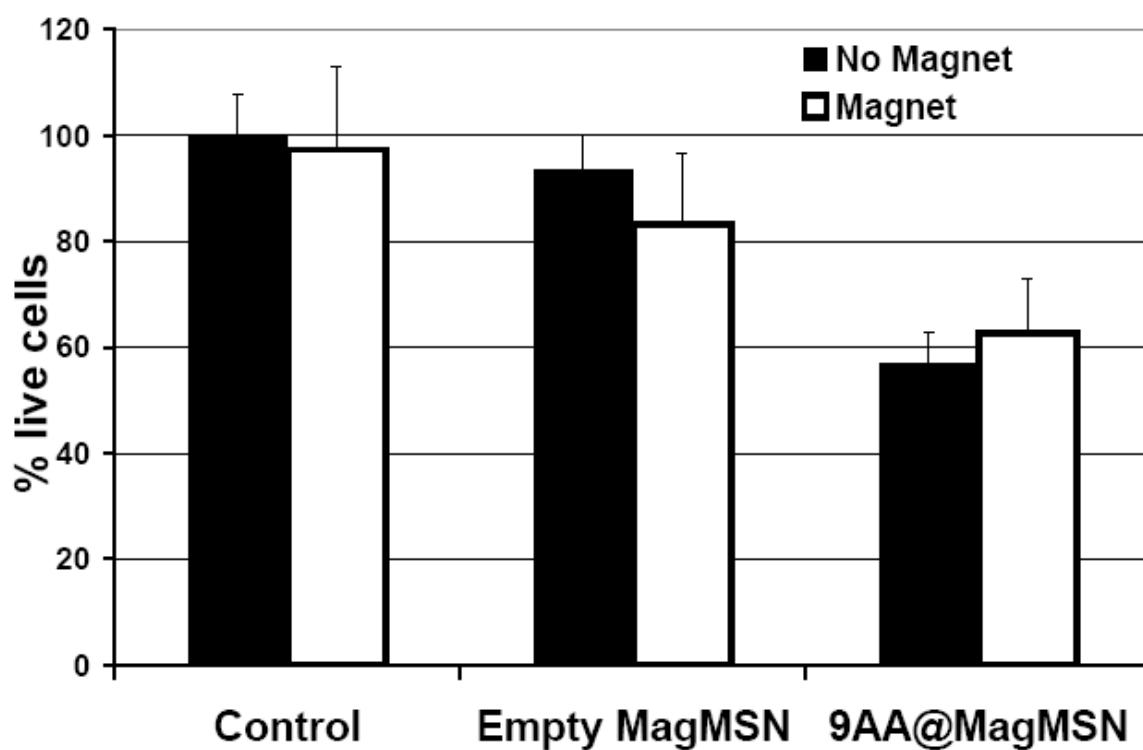


Figure 3. Viability experiments of HeLa cells after 2 days of incubation. The percentage of HeLa cells that were live has been plotted against the cell lines without any magnet-MSNs, cell lines with empty Magnet-MSNs and cell lines with 9AA loaded Magnet-MSNs shown from left to right respectively. The solid black bar represent the cell growth experiment in absence of a magnetic field and the white bars represents the same experiment in the presence of a strong (0.32 Tesla) magnetic field. The amount of both empty and 9AA loaded Magnet-MSN was $50.0 \mu\text{g mL}^{-1}$ of growth media.

In order to determine whether a strong magnetic field (0.32 Tesla surface field) has any effect on the HeLa cell growth, the same three cell culture experiments as described above were repeated by attaching a circular disk magnet (NdFeB, grade N50, 1.3 cm diameter) underneath each of the cell culture plate. No noticeable difference was observed after 2 days of incubation compared to the results obtained in the cases where no magnetic field was used (Figure 3). The findings of the above experiments suggest that a strong magnetic field (0.32 Tesla) does not have any effect on the growth of the HeLa cells either with or without the intracellular presence of Magnet-MSNs. It is also clear that the external magnetic field has no additional effect on the intracellular release of 9AA by assisting any uncapping process.

It is also very interesting to note that although the drug 9AA is a blue fluorescent molecule, no blue fluorescence was observed from the 9AA released inside the cell. We already observed and explained that the fluorescence of any fluorescent probe is not observed as long as those molecules stay inside the Magnet-MSN.⁸ However, the absence of fluorescence of the 9AA molecules that are released from the Magnet-MSN inside the cells is due to the quenching effect originating from the intercalation process with DNA. Kim et al. has quantified such quenching of fluorescence of 9AA due to intercalation with DNA in their published results.¹³

Conclusion

A successful demonstration of stimuli responsive intracellular delivery of a DNA intercalating drug 9-aminoacridine has been shown by magnetic nanoparticles capped MSNs that are taken up by HeLa cells possibly via endocytosis. The abundant presence of reduced

dihydrolipoic acid in HeLa cells was believed to trigger the release of drug molecules by reducing the disulfide linkage existing between the MSN and magnetic nanoparticles. Presence of a strong magnetic field did not have any significant effect on the intracellular delivery of the drug 9-aminoacridine. The superior efficiency of drug transfection using Magnet-MSNs was also successfully established by delivering the drug at concentration that was two orders of magnitude less than the concentration of the drug's actual LC_{50} value. In essence, we view that our Magnet-MSN system could pave a new approach towards magnetic field assisted targeted delivery of biomolecules into various cells and tissues.

Experimental section

APTS coated magnetite (Fe_3O_4) nanoparticles: Synthesis and coating of magnetic nanoparticles were performed following our published procedure.⁸

MCM-41-type mesoporous silica nanoparticles with 3-(propyldisulfanyl)propionic acid functionality (Linker-MSN): The Linker-MSN material was synthesized via our previously published procedure.⁸

Loading of 9AA in Magnet-MSN: Linker-MSN (15.0 mg) was dispersed in 4.0 mL of 9AA solution (1.13×10^{-4} M) in PBS (pH 7.4, 10 mM) and the mixture was stirred for a period of 24 h. In the next step, 1-[3-(dimethylamino)propyl]-3-ethylcarbodiimide hydrochloride (EDC, 45.0 mg) and APTS- Fe_3O_4 (170.0 mg) were added to the mixture and stirred for another 48 h. At the end, the mixture was filtered and washed with PBS and finally dried in the air. The filtrate was collected and analyzed for drug loading. The calculated loading of 9AA was found to be 5.3×10^{-6} mols g^{-1} of Linker-MSN, which is about 20.0 mole % loading.

Synthesis of empty Magnet-MSN (without 9AA): Linker-MSN (15.0 mg) was dispersed in 4.0 mL of 9AA solution (1.13×10^{-4} M) in PBS (pH 7.4, 10 mM) and the mixture was stirred for a period of 24 h. In the next step, 1-[3-(dimethylamino)propyl]-3-ethylcarbodiimide hydrochloride (EDC, 45.0 mg) and APTS-Fe₃O₄ (170.0 mg) were added to the mixture and stirred for another 48 h. At the end, the mixture was filtered and washed with PBS and finally dried in the air.

HeLa cell growth inhibition experiment: The cytotoxicity of Magnet-MSNs towards HeLa cells was studied using Guava ViaCount assay (Guava Technologies, Inc.; Hayward, CA). For that purpose HeLa cells were seeded in six well plates with a density of 1×10^5 cells mL⁻¹ in 3.0 mL of D-10 medium and allowed to attach for 24 h. After the attachment the supernatant media was replaced with D-10 media containing (a) no MSNs, (b) empty Magnet-MSNs and (c) 9AA loaded Magnet-MSN. After seeding them, the plates were set in an incubator at 37 °C and 5% CO₂. After 48 h incubation the plates were removed from the incubator, the media of each well was discarded, each well was washed with PBS solution, and the cells were then trypsinized, centrifuged and resuspended in D-10 medium. The cells in the resuspended media were then counted and their viability was determined by the Guava ViaCount cytometry assay.

References

- (1) Han, H. D.; Song, C. K.; Park, Y. S.; Noh, K. H.; Kim, J. H.; Hwang, T.; Kim, T. W.; Shin, B. C. *International Journal of Pharmaceutics* **2008**, *350*, 27-34.
- (2) Rapoport, N. *Progress in Polymer Science* **2007**, *32*, 962-990.

- (3) Nasongkla, N.; Shuai, X.; Ai, H.; Weinberg, B. D.; Pink, J.; Boothman, D. A.; Gao, J. *Angewandte Chemie, International Edition* **2004**, *43*, 6323-6327.
- (4) Stover, T. C.; Kim, Y. S.; Lowe, T. L.; Kester, M. *Biomaterials* **2007**, *29*, 359-369.
- (5) Hunter, A. C. *Advanced Drug Delivery Reviews* **2006**, *58*, 1523-1531.
- (6) Kwon, G. S.; Kataoka, K. *Advanced Drug Delivery Reviews* **1995**, *16*, 295-309.
- (7) Zhang, L.; Guo, R.; Yang, M.; Jiang, X.; Liu, B. *Advanced Materials (Weinheim, Germany)* **2007**, *19*, 2988-2992.
- (8) Giri, S.; Trewyn, B. G.; Stellmaker, M. P.; Lin, V. S. Y. *Angewandte Chemie, International Edition* **2005**, *44*, 5038-5044.
- (9) Hoffmann, G. R.; Calciano, M. A.; Lawless, B. M.; Mahoney, K. M. *Environmental and Molecular Mutagenesis* **2003**, *42*, 111-121.
- (10) Topal, M. D. *Biochemistry* **1984**, *23*, 2367-72.
- (11) Covey, J. M.; Kohn, K. W.; Kerrigan, D.; Tilchen, E. J.; Pommier, Y. *Cancer Research* **1988**, *48*, 860-865.
- (12) Biaglow, J. E.; Donahue, J.; Tuttle, S.; Held, K.; Chrestensen, C.; Mieyal, J. *Analytical Biochemistry* **2000**, *281*, 77-86.
- (13) Yoon, T.-J.; Kim, J. S.; Kim, B. G.; Yu, K. N.; Cho, M.-H.; Lee, J.-K. *Angewandte Chemie, International Edition* **2005**, *44*, 1068-1071.

CHAPTER 4. A MAGNETIC NANOPARTICLE ATTACHED PNIPAM POLYMER COATED MESOPOROUS SILICA NANOPARTICLE BASED HEAT RESPONSIVE DELIVERY SYSTEM USING ALTERNATING MAGNETIC FIELD AS STIMULI

A manuscript in preparation and to be submitted to *Angewandte Chemie*

Supratim Giri¹, Po-Wen Chung, Robert Vincent, Marek Pruski, Victor S. -Y. Lin²

Abstract

A polymer coated mesoporous silica nanomaterial (PNiPAm-MSN) was demonstrated to load and release drug molecules using thermal stimuli as a trigger. Iron oxide (Fe_3O_4) nanoparticles were attached to the surface of drug loaded PNiPAm-MSN to render the system magnetic (Mag-PNiPAm-MSN). Successful release of the loaded drug molecules was shown by placing Mag-PNiPAm-MSN under an alternating current based magnetic field. The mechanism of drug release was explained by the action of hyperthermia effect originating from the attached magnetic nanoparticles under the high frequency alternating magnetic field. The rate of drug release was also shown to be precisely controllable by controlling the parameters of the external magnetic field.

Introduction

In recent years, a great deal of attention has been paid in developing a delivery system for biomedical application that load and release a large amount of guest molecules.¹ Some of

¹ Primary researcher and author

² Author of correspondence

these systems show a stimuli responsive behaviour and have a controllable rate of release *in vitro*.²⁻⁶ However, once these materials go inside the cells the guest molecules are released in the cytosol or endosome either following the simple diffusion process⁷⁻⁹ or by the effect of any intracellular stimuli such as cell-produced antioxidants¹⁰ or by the change in intracellular pH¹¹ etc. So far it has not been possible to control the amount of the guest molecules once they start to come out from the delivery system inside the cells. Controlling the amount of guest molecules or drug release by any external stimuli poses a great challenge for controlled release therapy.

In this context, we have developed a mesoporous silica nanomaterial (MSN) based controlled release delivery system, where the amount of drug release can be controlled by an external magnetic field. The system utilizes the heating effect as a stimulus which is produced due to the presence of magnetic nanoparticles attached with the material under an alternating magnetic field, commonly known as hyperthermia.¹² As an external stimulus, magnetic field has proven to penetrate deep inside animal tissue.¹³⁻¹⁵ Hyperthermia properties of magnetic nanoparticles using alternating magnetic field has already been clinically employed to destroy cancer cells and tumours at a temperature (around 45 °C) far above than normal human body temperature.^{16,17} This high temperature also kills normal cells and damages healthy tissue. We designed a delivery system that is thermally responsive at a temperature range (38 °C – 40 °C) that is slightly above the normal human body temperature, yet not harmful enough to induce cell death or permanent tissue damage. We used a thermo-responsive polymer poly(*N*-isopropylacrylamide) commonly abbreviated as PNiPAm to coat the external surface of MSNs.¹⁸ The hydrophilic, random chain conformation of the external PNiPAm polymer layer on MSN surface at room temperature

acted as a soft cap and therefore allowed the MSN material to store drugs inside the mesoporous channels. A limited number of magnetic iron oxide (Fe_3O_4) nanoparticles were electrostatically attached on the surface of drug loaded PNiPAm coated MSNs. When these magnetic nanoparticles attached with drug loaded PNiPAm-MSN materials are placed in an alternating magnetic field, the heat energy generated due to the hyperthermia effect from the magnetic nanoparticles helps the PNiPAm polymer to change the conformation by raising the ambient temperature over the polymer's lower critical solution temperature (LCST). The change in the polymer conformation leads to uncapping of the pores and subsequent drug release is observed as shown by the scheme in Figure 1. The unique feature of this delivery

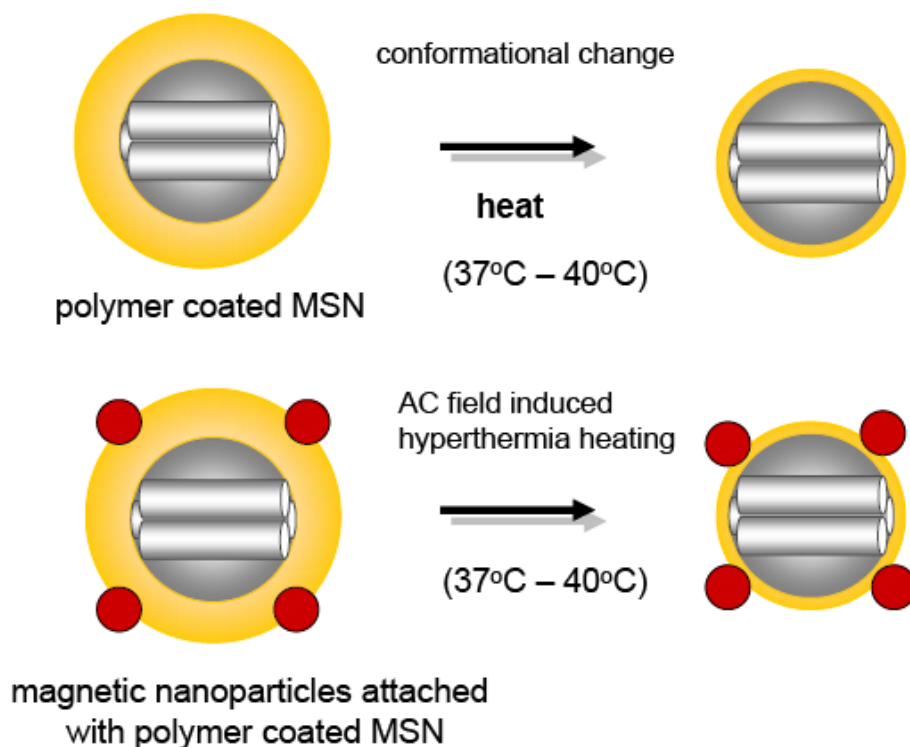


Figure 1. Scheme of stimuli responsive drug release based on the conformational change of PNiPAm polymer on MSN surface.

system is that, not only the drug release process can be turned ‘on’ or ‘off’ by the magnetic field, the rate and the amount of drug release can be precisely controlled by the heating effect, which is regulated by the intensity of the external magnetic field and time of exposure under the field. To the best of our knowledge, this is the first report that utilizes an external magnetic field to control drug release precisely from a bio-medical delivery system.

Results and discussion

We synthesized PNiPAm coated MSN from an aminopropyl functionalized MSN materials following our published procedure¹⁸ and termed as PNiPAm-MSN. The material consists of 200 nm sized MSN nanospheres coated with about 19 nm thick PNiPAm polymer layer as evident from transmission electron microscopy.¹⁸ Nitrogen sorption studies revealed that the surface area of PNiPAm-MSN material is about $600 \text{ m}^2 \text{ g}^{-1}$ which reflects the fact that the mesopores of the material are largely accessible for storing guest molecules and the chains of PNiPAm polymer grow from the outside of the pore surface and therefore do not block the pores to prevent entry of guest molecules.¹⁸ In order to test the drug loading capability of the PNiPAm-MSN, we used 9-aminoacridine (abbreviated as 9AA) as a model drug. The highly fluorescent, water soluble drug 9-aminoacridine is a well known DNA intercalator and a mutagen.^{19,20}

When PNiPAm-MSN was stirred in a solution of $1.3 \times 10^{-4} \text{ M}$ 9AA in PBS (pH 7.4, 10 mM) at room temperature, a considerable 9AA loading ($1.1 \times 10^{-5} \text{ moles g}^{-1}$ of PNiPAm-MSN) was observed (Table 1). Since water is an excellent promoter of intermolecular hydrogen bonding and 9AA is an aromatic amine, from the above experiment it is extremely difficult to figure out the location of the 9AA molecules with respect to MSN, *i.e.* whether

Table 1. Drug loading data

Material	Drug loading condition ^[a]		Loading of 9AA g ⁻¹ of material
	Step 1	Step 2	
PNiPAm-MSN	1.3×10 ⁻⁴ M 9AA in PBS stirred for 24 h at 25 °C	Resuspended in PBS for 48 h	1.1×10 ⁻⁵ moles
PNiPAm-MSN	1.3×10 ⁻⁴ M 9AA in THF stirred for 24 h at 25 °C	Resuspended in PBS for 48 h	7.0×10 ⁻⁶ moles
MSN (MCM-41)	1.3×10 ⁻⁴ M 9AA in THF stirred for 24 h at 25 °C	Resuspended in PBS for 48 h	3.0×10 ⁻⁸ moles

^[a]In the drug loading experiments, after step 1, the materials were filtered and washed. In step 2, the dried materials were further suspended in PBS (pH 7.4, 10mM) to drive out the physisorbed and leached out drug molecules from the materials. Drug loading calculations are done from the combined results of step 1 and step 2. For details see experimental section.

the drug molecules are inside the channels of MSN or they are out side the MSN being stuck with the PNiPAm polymer layer by forming intermolecular hydrogen bonding. To solve the ambiguity, the same drug loading experiment was carried out in THF (tetrahydrofuran), which is a polar aprotic solvent and does not promote intermolecular hydrogen bonding. Therefore the chances of the drug molecules getting attached to the polymer layer on the outside surface of MSN are very low in THF. It turned out that the loading of 9AA in THF under the same condition was 7.0×10⁻⁶ moles g⁻¹ of PNiPAm-MSN, which is little less than that was observed in PBS medium but still considerably high (Table 1). This considerably high drug loading in THF medium was attributed to the fact that PNiPAm-MSN material has a high accessible surface area (600 m²/g), which drives the 9AA molecules to diffuse inside the porous channels of MSN. The importance of high surface area of PNiPAm-MSN in drug loading was verified by a control experiment. Following Stober method,²¹ we synthesized

spherical colloidal silica with uniform diameter (300 nm) and coated those with PNiPAm polymer layer by the same synthetic procedure used in the case of PNiPAm-MSN. The resulting PNiPAm coated colloidal silica (termed as PNiPAm-SN) exhibited a surface area of $15 \text{ m}^2 \text{ g}^{-1}$ from nitrogen sorption studies. In the drug loading step, the exact same conditions were followed with 9AA in THF solution as in the case of PNiPAm-MSN. The observed 9AA loading was found to be 4.8×10^{-9} moles g^{-1} of PNiPAm-SN, which was clearly three orders of magnitude less than the loading of 9AA in PNiPAm-MSN. This experiment confirmed the importance of surface area in the drug loading using PNiPAm-MSN as host material.

Interestingly, when the 9AA loaded PNiPAm-MSN (3.0 mg) was dispersed in 2.0 mL of PBS (pH 7.4, 10 mM), less than 1% of loaded 9AA came out in the solution (Figure 2) at room temperature ($25 \text{ }^\circ\text{C}$) even after 36 h. On the contrary, when the same material (3.0 mg) was dispersed in 2.0 mL of THF at $25 \text{ }^\circ\text{C}$, majority (70%) of 9AA diffused out in the solution (not shown in the figure) after same time. The above observation can be explained in the light of intermolecular hydrogen bonding between 9AA and PNiPAm polymer chain. When PNiPAm-MSN is dispersed in PBS, 9AA molecules are unable to come out from the pores, owing to the favourable intermolecular hydrogen bonding with the polymer layer in aqueous medium at room temperature. This effect becomes insignificant when the dispersion medium is changed to THF, lack of intermolecular hydrogen bonding between the polymer and the drug leads to diffusion of 9AA molecules from the mesopores of MSN into the dispersion medium. This suggests that in aqueous medium at $25 \text{ }^\circ\text{C}$, the PNiPAm layer acts as a gate keeping layer for 9AA loaded in MSN. We rationalize the entire drug loading and retention

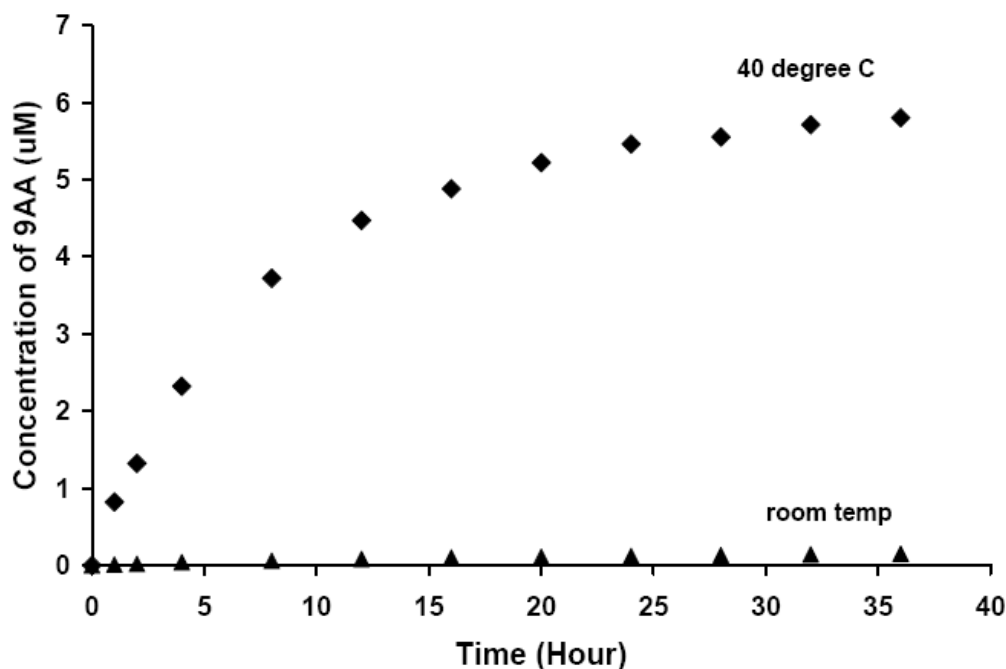


Figure 2. Release plot of 9AA from PNiPAm-MSN (3.0 mg) in PBS (2.0 mL, pH 7.4, 10 mM).

behaviour by PNiPAm-MSN in the following way- the high surface area of MSN invites the drug molecules inside the channels of MSN and the gate keeping effect of PNiPAm polymer layer prevents them to leach out in aqueous medium at room temperature by the effect of intermolecular hydrogen bonding. This rationale is further corroborated by another control experiment. Bare MSNs (MCM-41 type with no PNiPAm coating) having the same size and morphology as of PNiPAm-MSNs were loaded with 9AA in THF following the same drug loading conditions (Table 1) and a two orders of magnitude less drug loading is observed compared to the drug loading in the case of PNiPAm-MSN. This control experiment clearly indicates that without the screening of PNiPAm polymer layer, it is not possible to retain the drugs inside the channels of MSN in aqueous medium.

A notably important phenomenon was observed when the temperature of the PBS (2.0 mL) medium containing 9AA (loaded in THF) loaded PNiPAm-MSN (3.0 mg) was raised to 40°C by a controlled oil bath heating. More than half (55%) of loaded 9AA was released following a typical diffusion pattern within 36 h (Figure 2). As the lower critical solution temperature (LCST) of the PNiPAm polymer typically lies in the range of 32 °C - 33 °C, the side chains of the polymer undergoes a major conformational change at a temperature of about 40 °C and higher. The side chains of PNiPAm form extensive intramolecular hydrogen bonding with each other and thereby become hydrophobic and collapse in the form of globules. This temperature assisted collapse of the polymer screen induces the drug release from the mesopores of PNiPAm-MSNs.

As the PNiPAm-MSN system is capable of releasing drugs when subjected to thermal stimuli, we tried to modify the system further to incorporate magnetic nanoparticles on the surface of the materials so that the magnetic field based controlled hyperthermia can be employed to develop a precisely magnetic field responsive delivery system. To attach magnetic nanoparticles on the surface of 9AA loaded PNiPAm-MSN, we followed the same drug loading procedure at room temperature in THF medium that has been already described. After vortexing PNiPAm-MSN (30 mg) in 1.3×10^{-4} M 9AA in THF at room temperature for 24 h, aminopropylsiloxane functionalized Fe₃O₄ nanoparticles (APTS-Fe₃O₄, 45 mg) with an average diameter of 10 nm were added into the solution and stirred for another 24 h. The aminopropyl functional group on the surface of magnetic nanoparticles enable them to be monodispersed and of uniform size and shape. After the isolation of the final material, a limited number of magnetic Fe₃O₄ nanoparticles were found to be attached on the surfaces of 9AA loaded PNiPAm-MSN particles as evident from the transmission electron micrograph

(Figure 3). We believe that the mode of attachment between the PNiPAm-MSN and Fe_3O_4 nanoparticles is electrostatic in nature where the former being negatively charged and the later being positively. Due to the presence of magnetic nanoparticles on the surface of PNiPAm-MSN, the entire material became magnetic and the obtained 9AA loaded material is termed as Mag-PNiPAm-MSN. The loading of 9AA in this case was found to be 7.0×10^{-6} moles of 9AA/g of PNiPAm-MSN, which is the same value for the loading of 9AA in THF for PNiPAm-MSN itself. This suggests that the presence of a limited number of magnetic nanoparticles on the surface of PNiPAm-MSN did not interfere with drug loading.

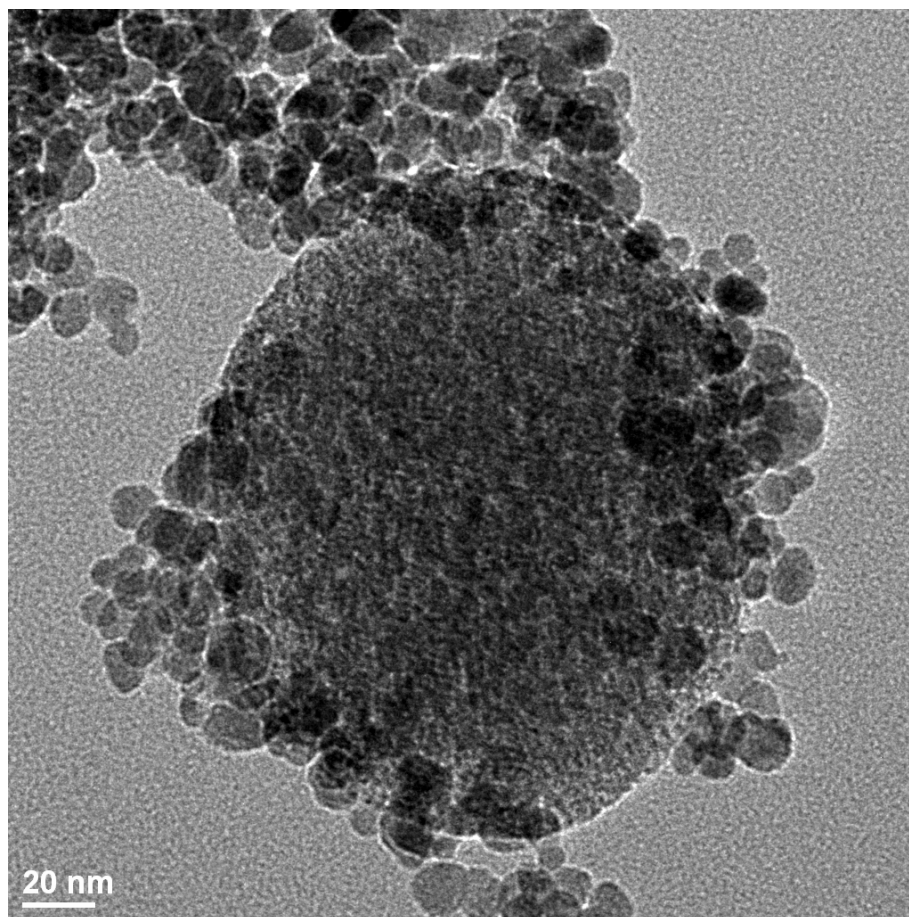


Figure 3. Transmission electron micrograph of Mag-PNiPAm-MSN.

In order to demonstrate that the drug loaded Mag-PNiPAm-MSN is still capable of releasing drug molecules when subjected to thermal stimuli, we carried out another simple *in vitro* experiment. When 9AA loaded Mag-PNiPAm-MSN is suspended in PBS medium, a similar less than 1% release of 9AA in the solution is observed over a period of after 36 h indicating the capping efficiency of the system remained intact (Figure 4). The material (Mag-PNiPAm-MSN) also showed similar thermal stimuli responsive behaviour by releasing a 32% of loaded 9AA in the solution following a similar diffusional pattern when temperature of the PBS solution containing Mag-PNiPAm-MSN was raised to 40 °C by controlled oil bath heating. This indicated that the presence of a limited number of magnetic

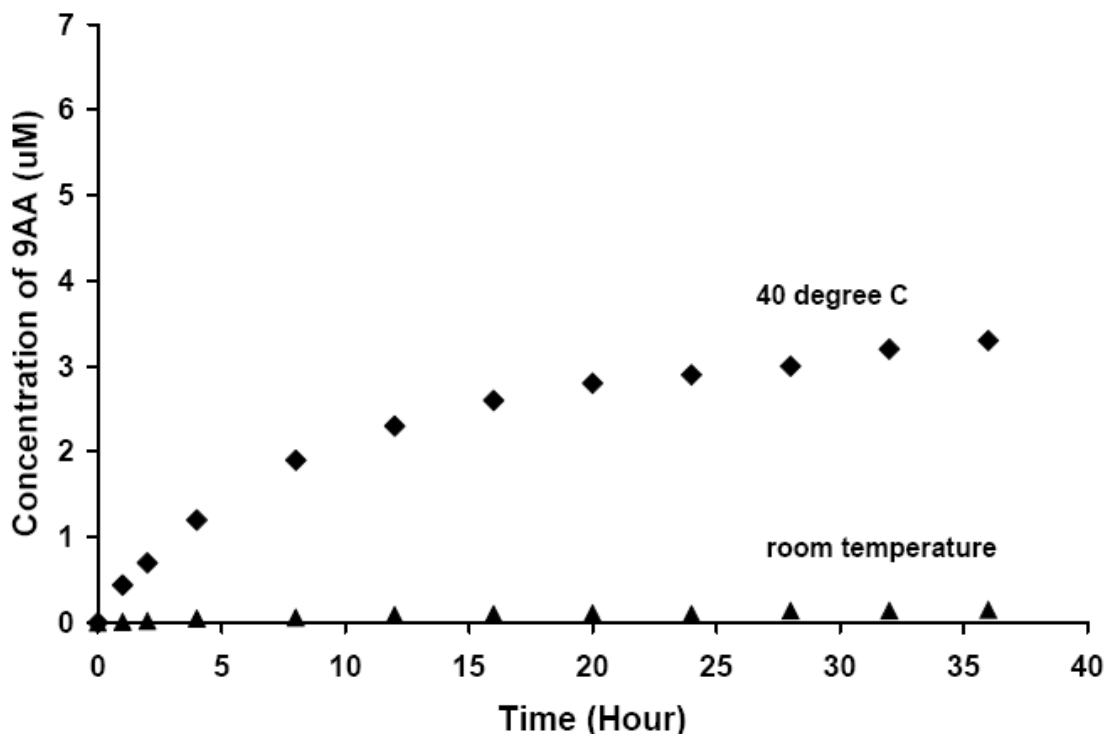


Figure 4. Release plot of 9AA from Mag-PNiPAm-MSN (7.5 mg) in PBS (2.0 mL, pH 7.4, 10 mM).

nanoparticles on the surface of PNiPAm-MSN material did not hinder the release of 9AA much, yet the presence of the magnetic nanoparticle rendered PNiPAm-MSN magnetic and magnetic property can readily be exploited to target the material to a point of interest by a magnetic field and using the alternating magnetic field as a stimulus, a drug release can be triggered and the rate of release can be regulated precisely.

To utilize the alternating magnetic field induced heating effect using Mag-PNiPAm-MSN, we fabricated a prototype electromagnetic device in our laboratory. An AC source was connected to a power amplifier which was connected to an electromagnetic coil (Figure 5). The power amplifier is able to control the frequency of the input AC signal from 50 kHz to 1 MHz and is also able to control the root mean square (RMS) voltage across the coil. When a current passes across the electromagnetic coil there is a magnetic field generated in the centre of the coil acting in the longitudinal direction. According to the theory of electromagnetism, the intensity of the magnetic field produced (H) depends on the number of turns in the coils

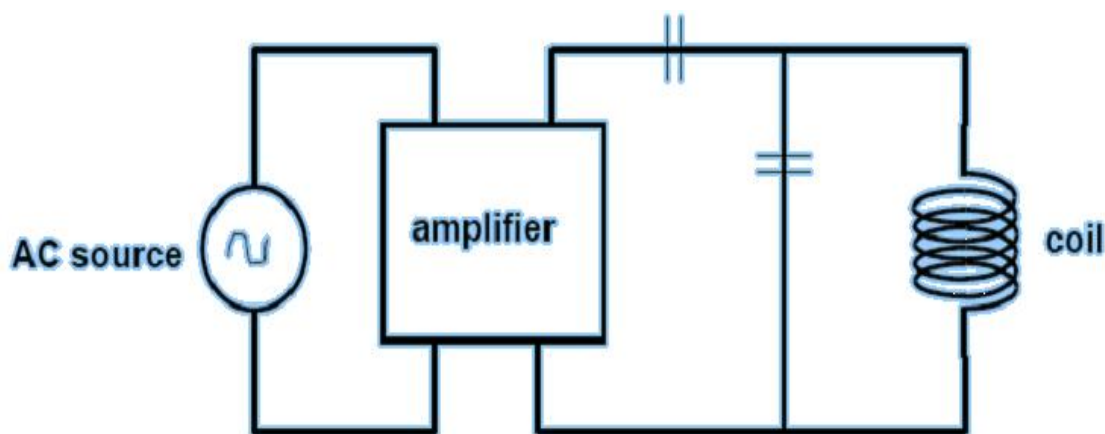


Figure 5. Simplified circuit diagram of the electromagnetic device used for hyperthermia experiment.

(N) and the current (I) passing through the coil. Intensity of the magnetic field (H) increases with I for a given coil (constant N). An AC voltage can be written as following:

$$\text{AC voltage: } V(t) = V_{\text{peak}} \text{ Sin}(2\pi f.t) \quad [f = \text{frequency (Hz)}]$$

The AC voltage across the electromagnetic coil is usually expressed in its RMS value [$V_{\text{RMS}} = V_{\text{peak}}/\sqrt{2}$]. In other words, higher the V_{RMS} across the coil, higher is the current (I) passing through the coil and higher will be the intensity (H) of the magnetic field. As the current changes the direction following its corresponding AC frequency, the direction of the magnetic field (H) also changes according to the same frequency and this leads to the formation of an alternating magnetic field inside the coil. When magnetic nanoparticles are placed within this alternating magnetic field, heat energy is produced by a phenomenon commonly known as hyperthermia.¹² There are two theories that rationalize the effect of hyperthermia known in the literatures. One of the major theories is the theory of Neel relaxation which states that the magnetic moments of the individual particles under an alternative magnetic field rotate while the particles remain stationary and the energy (supplied by the external AC magnetic field) is dissipated into heat energy when the particle relaxes into its equilibrium orientation.²² According to the second theory, that is the theory of Brownian motion, rotation of the particles also take place due to the torque exerted on the magnetic moment by the external AC magnetic field and the rotational energy due to Brownian motion is transformed into heat energy.²² In order to demonstrate that our electromagnetic device can produce heat from magnetic nanoparticle by the hyperthermia process, we performed an experiment (Table 2). We suspended APTS-Fe₃O₄ (20 mg) in a vial containing 2 mL PBS (pH 7.4, 10 mM) and exposed it under AC magnetic field (110 V_{RMS}) for 6 minutes for three different frequencies 400 kHz, 800 kHz and 1 MHz, one at a

Table 2. Effect of hyperthermia using alternating magnetic field

Coil frequency (kHz)	RMS voltage across coil (V)	Exposure time (min)	Temperature ^[a] of 20 mg APTS-Fe ₃ O ₄ in 2 mL PBS (°C)	Temperature ^[a] of 2 mL PBS [Control] (°C)
400	110	6	35	33
800	110	6	36	34
1000	110	6	40	34

^[a] Starting temperature is 25 °C

time. The temperature of the solution containing magnetic nanoparticles was raised to 35 °C, 36 °C and 40 °C from 25 °C for the frequencies 400 kHz, 800 kHz and 1 MHz respectively. We also did a control experiment where a vial containing 2 mL PBS (without any magnetic nanoparticles) was subjected to the same experimental conditions and the temperature of the solution was raised to 33°C, 34°C and 34°C (initial temperature was 25 °C) for the frequencies 400 kHz, 800 kHz and 1 MHz respectively. The difference of heating effect between magnetic nanoparticles containing solution and the blank control solution reflects the effect of hyperthermia. The temperature elevation of the control solution was attributed to the inherent heating effect of the magnetic coil due to electrical resistance.

The parameters obtained from the previous experiment (as shown in Table 2) were followed to demonstrate the hyperthermia triggered drug release effect from 9AA loaded Mag-PNiPAm-MSN. A vial containing Mag-PNiPAm-MSN (7.5 mg) suspended in 2 mL PBS (pH 7.4, 10 mM) was placed inside a magnetic coil which is capable of operating at a frequency of 1 MHz. A less than 1% release of 9AA was observed at room temperature when no magnetic field was applied and the plot was termed as zero field release (Figure 6). The magnetic field corresponding to an RMS voltage of 110 V was turned on at point A. The

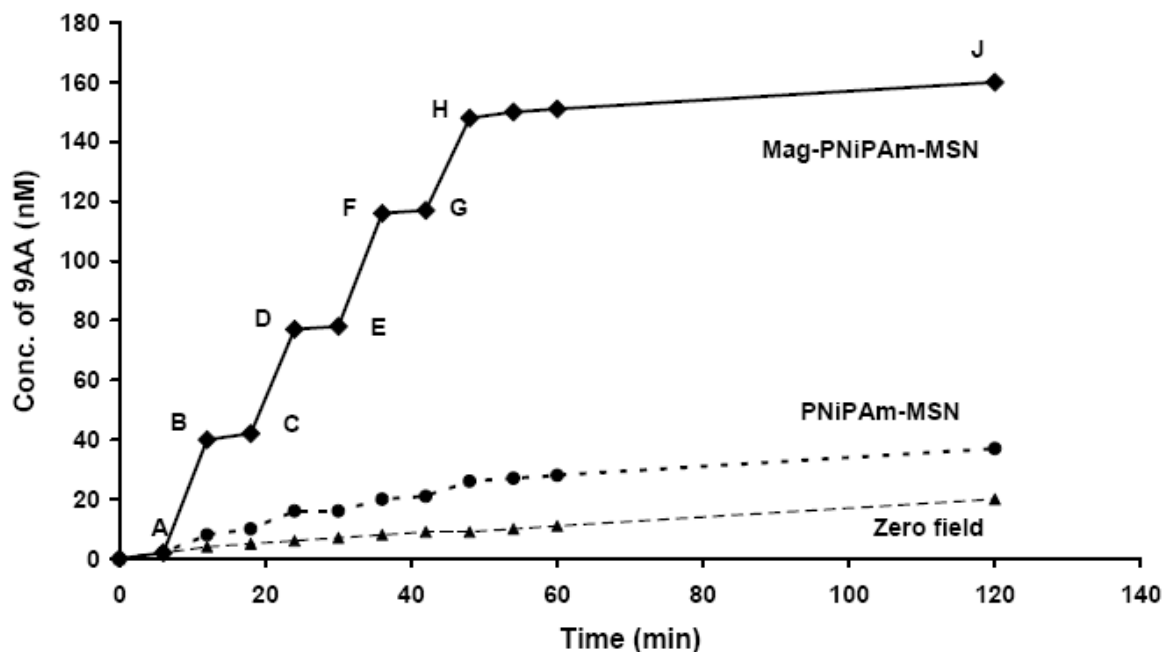


Figure 6. Role of magnetic nanoparticles on the PNiPAm-MSN surface in the release of 9AA due to magnetic field trigger corresponding to an RMS voltage of 110 V, and 1 MHz AC frequency.

material was exposed under magnetic field for a period of 6 min and after 6 min the field was turned off and the immediate measurement of 9AA released in the solution was plotted in point B. A sharp increase (42 nM) in the concentration of released 9AA was observed from point A to B due to the magnetic field trigger. A period of another 6 min was maintained in the absence of magnetic field and at point C, the released concentration was found to be almost the same as point B. The same cycle of experiment was continued in a successive manner from point C to point H and a step wise release of 9AA was observed only during the time the material was kept exposed under magnetic field. When the magnetic field was kept off for a longer period, almost no release of 9AA from Mag-PNiPAm-MSN was observed as plotted from point H to point J. To estimate the effect of 9AA release due to the inherent

heating of the magnetic coil itself, the same step wise release experiment was done on PNiPAm-MSN (without any magnetic nanoparticles). The release of 9AA in this case was much less than that from Mag-PNiPAm-MSN and very close to the zero field control release as seen in the plot (Figure 6). These results indicate that the presence of magnetic nanoparticles on the surface of PNiPAm-MSN makes the delivery system responsive towards alternating magnetic field based hyperthermia induced drug release and the heating effect from the coil itself does not have any considerable effect on the release.

We also conducted a prolonged experiment to determine the maximum amount of 9AA release from Mag-PNiPAm-MSN using the same 6 min exposure followed by 6 min interval process and the maximum possible release was found to be about 5% of total 9AA loaded and about 18% of the maximum amount of 9AA released in the case of oil bath heating at 40 °C (Figure 7).

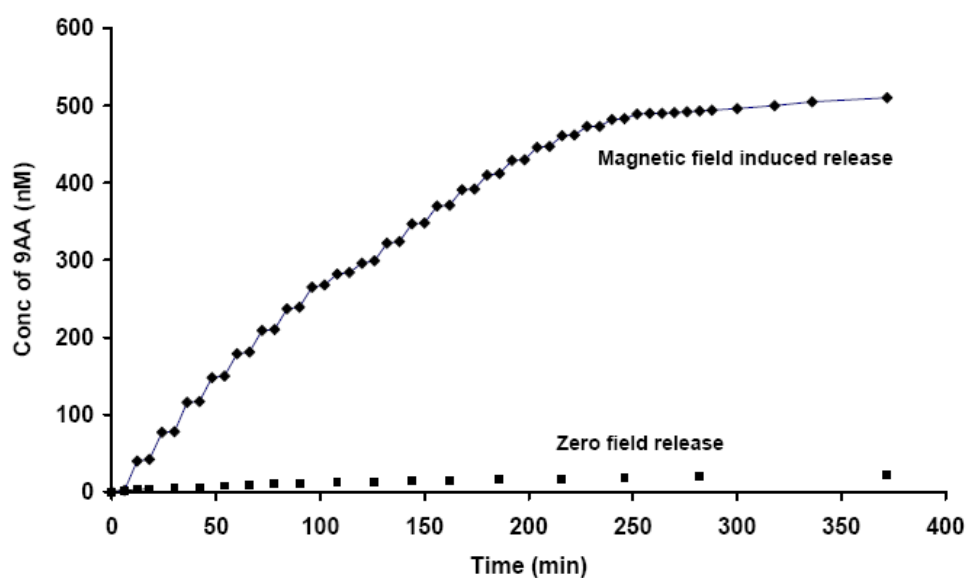


Figure 7. Release of 9AA from Mag-PNiPAm-MSN under prolonged experiment of 6 min magnetic field exposure followed by 6 min of interval in successive manner.

We also demonstrated that the release of 9AA is indeed responsive to the duration of magnetic field exposure, the voltage across the coil (V_{RMS}) and the frequency of the alternating magnetic field (Figure 8a-d). We observed a 78 nM release of 9AA in the PBS (2.0 mL, pH 7.4, 10 mM) when Mag-PNiPAm-MSN (7.5 mg) was subjected to a 1MHz magnetic field with 110 V_{RMS} after two complete cycles of 6 min exposure followed by 6 min interval experiment (Figure 8a). The same experiment was done with a 12 min exposure

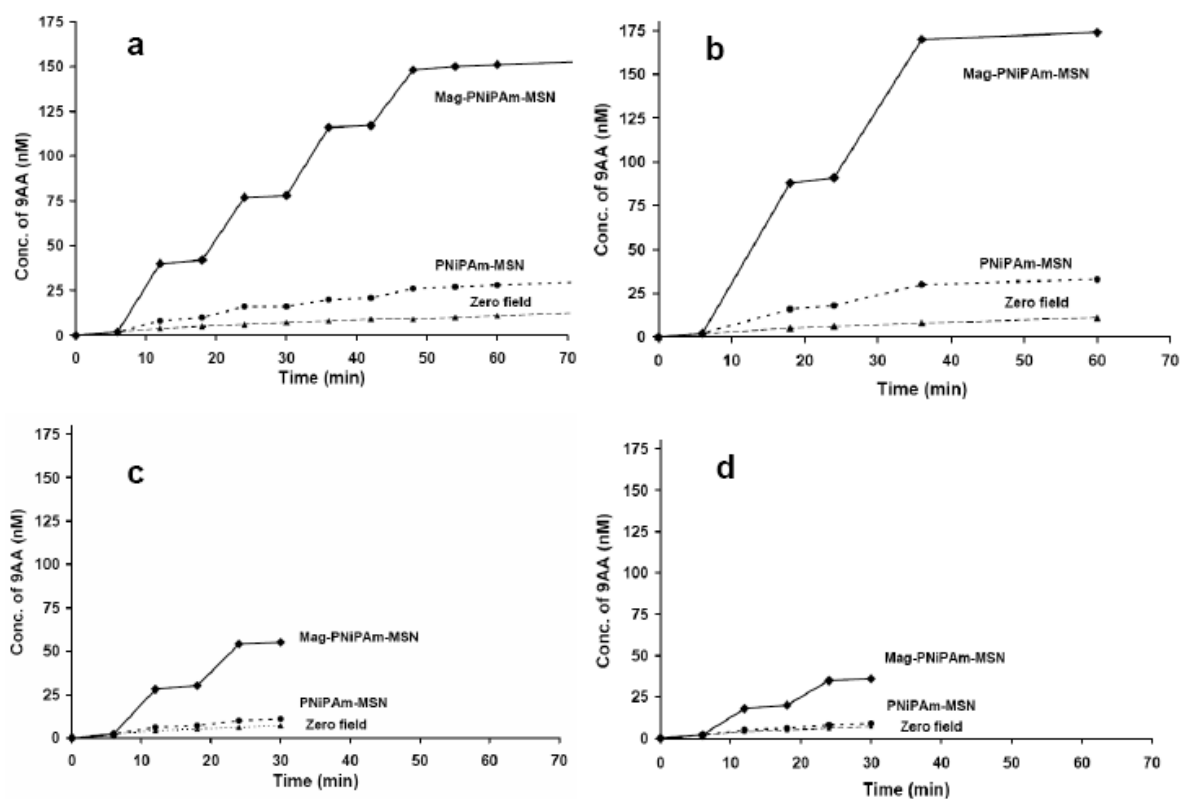


Figure 8. Controlled release of 9AA by varying time of exposure, intensity of the magnetic field (RMS voltage) and frequency of the alternating magnetic field, (a) exposure time 6 min, 110 RMS volt and 1 MHz AC frequency (b) exposure time 12 min, 110 RMS volt and 1 MHz AC frequency (c) exposure time 6 min, 65 RMS volt and 1 MHz AC frequency (d) exposure time 6 min, 65 RMS volt and 800 kHz AC frequency. For the values of the intensities of the magnetic field (H) see experimental section.

followed by 6 min interval process and after two complete cycles, the concentration of the released 9AA was found to be 170 nM (Figure 8b). In the next experiment, the voltage across the coil (V_{RMS}) was reduced to 65 V keeping the frequency same (1 MHz) and the process of 6 min exposure followed by 6 min interval was carried out. The release of 9AA was found to be 56 nM after two complete cycles (Figure 8c) in this case. The release was also possible to keep at a lower value (38 nM) by switching to a lower frequency of 800 kHz (Figure 8d).

It is interesting to note that in all the above magnetic field induced release experiments discussed so far, the release is measured before the application of the magnetic field and at the end of the field exposure. Therefore, the release plot appears as a step wise profile. Although, Hu et al. has reported a similar step wise release of drug from magnetic nanoparticle embedded silica systems by an alternating magnetic field,²³ we tried to investigate the real nature of the 9AA release during the time Mag-PNiPAm-MSN is exposed under the magnetic field (Figure 9). We suspended Mag-PNiPAm-MSN (7.5 mg) in 2 mL PBS (pH 7.4, 10 mM) and placed inside a magnetic coil operating at a frequency of 1 MHz. In the absence of magnetic field, almost no release of the 9AA was observed for the first 6 min up to point A. At point A the magnetic field corresponds to 110 RMS volt was applied for next 12 min up to point B. During this 12 min of exposure, release of 9AA was monitored in every two minutes. We observed a gradual increase of release of 9AA during the exposure under magnetic field. As soon as the field is withdrawn at point B, almost no further release is observed from point B to point C (Figure 9). The same cycle was repeated at point C and the same result was obtained. This type of continuous release of drug molecules assisted by the magnetic field mediated hyperthermia was also reported by Babincova et al. with their liposome coated magnetic nanoparticle systems.²⁴

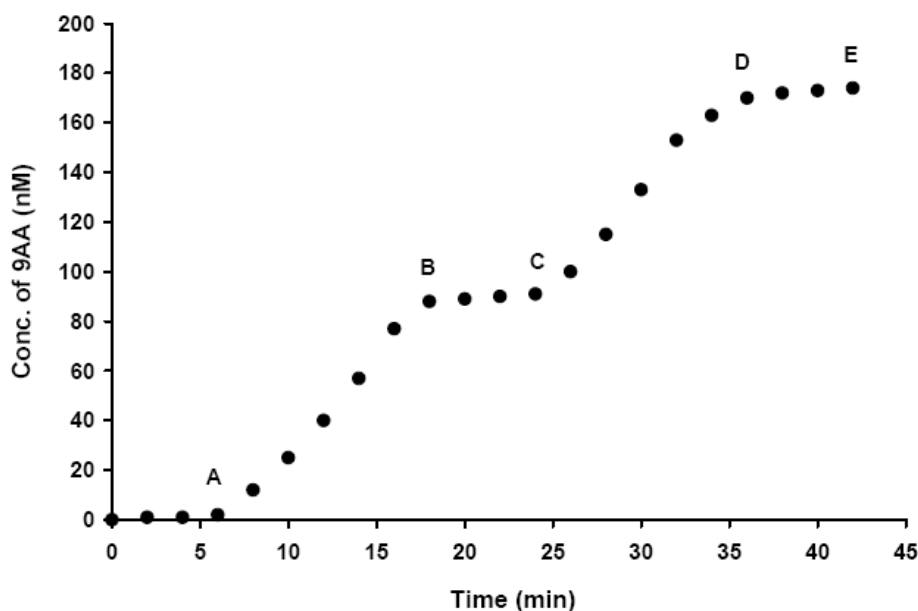


Figure 9. Release of 9AA from Mag-PNiPAm-MSN as a function of time, triggered by magnetic field. The release of 9AA is measured in every 2 min during the exposure under alternating magnetic field corresponds to a frequency of 1 MHz at an RMS voltage of 110 V.

Conclusion

In conclusion, we have demonstrated that PNiPAm polymer coated mesoporous silica attached with magnetic iron oxide nanoparticles – so-called Mag-PNiPAm-MSNs – can be used as an alternating magnetic field stimuli-responsive controlled-release delivery carrier. Drug molecules that are stored within the pores of the materials can be released by turning on the magnetic field and release can be turned off by switching the magnetic field off. We believe the mechanism of drug release behaviour is controlled by the conformational change of the PNiPAm polymer regulated by the hyperthermia effect coming from the attached magnetic nanoparticles. The unique feature of this delivery system is that the rate of the drug release can precisely controlled by tuning the three physical parameters of the external magnetic field stimuli, which are the voltage across the magnetic coil (controls the intensity

of the magnetic field), duration time the material being exposed under the magnetic field and the frequency of the alternating magnetic field. We envision that these Mag-PNiPAm-MSNs could play a significant role in the development of a delivery system that will control the intracellular release of guest molecules.

Experimental section

Synthesis of PNiPAm-MSN: Synthesis of PNiPAm polymer coated MSN was carried out following our previously published literature.¹⁸

Synthesis of 3-aminopropyltrimethoxysilane coated Fe₃O₄ (APTS-Fe₃O₄): Synthesis of magnetic nanoparticles (APTS-Fe₃O₄) was followed by our previously published literature.¹⁰

Synthesis of colloidal silica: Synthesis of colloidal silica was carried out by following Stober method.²¹ Ethanol (92.0 mL), ammonium hydroxide (26.0 mL) and distilled water (92.0 mL) were mixed and magnetically stirred for 5 min in an Erlenmeyer flask. In the next step, tetraethyl orthosilicate (10.0 mL) was added to the mixture at a constant rate of 10 mL/min followed by sealing and the stirring of the solution for 3 h. The suspension was then centrifuged at a speed of 1800 rpm and the supernatant was decanted. The resulting solid was then washed with distilled water followed by sonication and centrifugation. The process was repeated twice and finally the material was dried into white powder.

Synthesis of PNiPAm coated colloidal silica: Colloidal silica (1.0 g) synthesized from the above procedure, was dispersed in anhydrous toluene (80.0 mL) and 3-aminopropyltrimethoxysilane (1 mmol) was added to the mixture followed by reflux at 80°C for 8 h in the first step. At the end, the suspension was cooled down, centrifuged and washed

with toluene, followed by water and ethanol, respectively. The material (AP-SN) was finally dried to obtain aminopropyl grafted colloidal silica (AP-SN). In the second step, AP-SN (150 mg) was reacted with 3-benzylsulfanyl-thiocarbonylsufanylpropionic acid (61.3 mg) in the presence of *N*-Ethyl-*N'*-(3-dimethylaminopropyl)carbodiimide (EDC; 42.0 mg) in 8.0 mL methylene chloride at room temperature for 24 h. After the reaction, the solution was filtered and the particles were washed by copious amount of methylene chloride and methanol to remove the physisorbed RAFT (reversible addition-fragmentation chain transfer) agents. The resulting material was dried under vacuum overnight to obtain RAFT-SN as a dry yellowish powder. In the third and final step, RAFT-SN (100.0 mg), azobisisobutyronitrile (0.3 mg), *N*-isopropylacrylamide (1.13 g), and DMF (5.0 mL) were mixed in a Schlenk tube, followed by sonication for 5 min. The tube was subjected to three cycles of freeze-pump-thaw degas process to remove oxygen. The tube was then placed in an oil bath preset at 70°C for 24 h. The polymerization was terminated by opening the tube to atmosphere and then diluted with methanol. The resulting PNiPAm coated colloidal silica was obtained by centrifuging the solution. The solid product was isolated by filtration and washed with copious amount of methanol to remove any unreacted monomers and physisorbed NiPAm polymer.

Loading of 9-aminoacridine (9AA) inside PNiPAm-MSN in THF: In the first step, PNiPAm-MSN (30.0 mg) was suspended in 3.0 mL solution of 9AA in THF (1.3×10^{-4} M) and the mixture was stirred for 24 h at room temperature. At the end, the suspension was filtered, washed several times with THF and residue was dried into powder. The filtrate was collected. In the second step, the dried powder residue was again suspended in 3.0 mL PBS (pH 7.4, 10 mM) at room temperature for 48 h. The number of moles of 9AA found in the

filtrate and the number of moles of 9AA leaked out in the PBS in second step was added and this total number of moles was then subtracted from the initial number moles of 9AA used in the first step to obtain the net 9AA loading, which was found to be 7.0×10^{-6} moles/g of PNiPAm-MSN and that corresponds to 54.0 mole% loading.

Loading of 9-aminoacridine (9AA) inside bare MSN (MCM-41 type) in THF: In the first step, bare MSN (30.0 mg) was suspended in 3.0 mL solution of 9AA in THF (1.3×10^{-4} M) and the mixture was stirred for 24 h at room temperature. At the end, the suspension was filtered, washed several times with THF and residue was dried into powder. The filtrate was collected. In the second step, the dried powder residue was again suspended in 3.0 mL PBS (pH 7.4, 10 mM) at room temperature for 48 h. The number of moles of 9AA found in the filtrate and the number of moles of 9AA leaked out in the PBS in second step was added and this total number of moles was then subtracted from the initial number moles of 9AA used in the first step to obtain the net 9AA loading, which was found to be 3.0×10^{-8} moles/g of MSN and that corresponds to 0.23 mole% loading.

Loading of 9-aminoacridine (9AA) inside PNiPAm coated colloidal silica in THF: In the first step, PNiPAm coated colloidal silica (30.0 mg) was suspended in 3.0 mL solution of 9AA in THF (1.3×10^{-4} M) and the mixture was stirred for 24 h at room temperature. At the end, the suspension was filtered, washed several times with THF and colloidal silica was dried into powder. The filtrate was collected. In the second step, the dried powder residue was again suspended in 3.0 mL PBS (pH 7.4, 10 mM) at room temperature for 48 h. The number of moles of 9AA found in the filtrate and the number of moles of 9AA leaked out in the PBS in second step was added and this total number of moles was then subtracted from

the initial number moles of 9AA used in the first step to obtain the net 9AA loading, which was found to be 4.8×10^{-9} moles of 9AA/g of PNiPAm coated colloidal-silica.

Loading of 9-aminoacridine (9AA) inside Mag-PNiPAm-MSN in THF: In the first step, PNiPAm-MSN (30.0 mg) was suspended in 3.0 mL solution of 9AA in THF (1.3×10^{-4} M) and the mixture was stirred for 24 h at room temperature, followed by addition of APTS- Fe_3O_4 (45 mg) *in situ* and the whole mixture was stirred for another 24 h. At the end, the suspension was filtered, washed several times with THF and the residue was dried into powder. The filtrate was collected. In the second step, the dried powder residue was again suspended in 3.0 mL PBS (pH 7.4, 10 mM) at room temperature for 48 h. The number of moles of 9AA found in the filtrate and the number of moles of 9AA leaked out in the PBS in second step was added and this total number of moles was then subtracted from the initial number moles of 9AA used in the first step to obtain the net 9AA loading, which was found to be 7.0×10^{-6} moles/g of PNiPAm-MSN.

Measurement of the concentration of 9-aminoacridine: Standard solutions of 9AA were made in PBS (pH 7.4, 10 mM) and in THF. The fluorescence intensities of the corresponding standard 9AA solutions were recorded using the fluoremeter and standard calibration curves were obtained by plotting the fluorescence intensity maxima at 429 nm (excitation wavelength was 343 nm) versus various concentrations.

Experimental setup of the electromagnetic device: The circuit used to setup the electromagnetic device is shown in simplified form in Figure 5. Several electromagnetic coils that were capable of working with AC frequency in the range of 50 kHz to 1 MHz with variable inductance were also built. Each of the coils was made with copper wires with a constant internal coil diameter of 12 mm. The coils were the elements of a resonant RLC

circuit with a variable capacity in the range of 600 pF to 20 nF and were capable to produce a magnetic field (H) intensity up to 2.0 kAm^{-1} . The inductance of 1 MHz coil was 20 μH with the coil quality factor of 17.5. The intensity of the magnetic field (H) for 1 MHz coil was 1.25 kAm^{-1} when the corresponding RMS was 110 V and was 0.8 kAm^{-1} when the corresponding RMS was 65 V. The value of H for 800 kHz coil was 0.85 kAm^{-1} with the corresponding 65 V RMS.

References

- (1) Giri, S.; Trewyn, B. G.; Lin, V. S. Y. *Nanomedicine (London, United Kingdom)* **2007**, *2*, 99-111.
- (2) Lai, C.-Y.; Trewyn, B. G.; Jeftinija, D. M.; Jeftinija, K.; Xu, S.; Jeftinija, S.; Lin, V. S. Y. *Journal of the American Chemical Society* **2003**, *125*, 4451-4459.
- (3) Mal, N. K.; Fujiwara, M.; Tanaka, Y. *Nature (London, United Kingdom)* **2003**, *421*, 350-353.
- (4) Nguyen, T. D.; Tseng, H.-R.; Celestre, P. C.; Flood, A. H.; Liu, Y.; Stoddart, J. F.; Zink, J. I. *Proceedings of the National Academy of Sciences of the United States of America* **2005**, *102*, 10029-10034.
- (5) Casasus, R.; Marcos, M. D.; Martinez-Manez, R.; Ros-Lis, J. V.; Soto, J.; Villaescusa, L. A.; Amoros, P.; Beltran, D.; Guillem, C.; Latorre, J. *Journal of the American Chemical Society* **2004**, *126*, 8612-8613.
- (6) Yang, Q.; Wang, S.; Fan, P.; Wang, L.; Di, Y.; Lin, K.; Xiao, F.-S. *Chemistry of Materials* **2005**, *17*, 5999-6003.

- (7) Slowing, I. I.; Trewyn, B. G.; Lin, V. S. Y. *Journal of the American Chemical Society* **2007**, *129*, 8845-8849.
- (8) Shah, L. K.; Amiji, M. M. *Pharmaceutical Research* **2006**, *23*, 2638-2645.
- (9) Oishi, M.; Hayashi, H.; Iijima, M.; Nagasaki, Y. *Journal of Materials Chemistry* **2007**, *17*, 3720-3725.
- (10) Giri, S.; Trewyn, B. G.; Stellmaker, M. P.; Lin, V. S. Y. *Angewandte Chemie, International Edition* **2005**, *44*, 5038-5044.
- (11) Das, M.; Mardyani, S.; Chan, W. C. W.; Kumacheva, E. *Advanced Materials (Weinheim, Germany)* **2006**, *18*, 80-83.
- (12) Fortin, J.-P.; Wilhelm, C.; Servais, J.; Menager, C.; Bacri, J.-C.; Gazeau, F. *Journal of the American Chemical Society* **2007**, *129*, 2628-2635.
- (13) Hilger, I.; Andra, W.; Hergt, R.; Hiergeist, R.; Schubert, H.; Kaiser, W. A. *Radiology FIELD Full Journal Title:Radiology* **2001**, *218*, 570-5.
- (14) Hilger, I.; Hergt, R.; Kaiser, W. A. *Journal of Magnetism and Magnetic Materials* **2005**, *293*, 314-319.
- (15) Kawai, N.; Ito, A.; Nakahara, Y.; Futakuchi, M.; Shirai, T.; Honda, H.; Kobayashi, T.; Kohri, K. *Prostate (Hoboken, NJ, United States)* **2005**, *64*, 373-381.
- (16) Jordan, A.; Scholz, R.; Maier-Hauff, K.; Johannsen, M.; Wust, P.; Nadobny, J.; Schirra, H.; Schmidt, H.; Deger, S.; Loening, S.; Lanksch, W.; Felix, R. *Journal of Magnetism and Magnetic Materials* **2001**, *225*, 118-126.
- (17) Drake, P.; Cho, H.-J.; Shih, P.-S.; Kao, C.-H.; Lee, K.-F.; Kuo, C.-H.; Lin, X.-Z.; Lin, Y.-J. *Journal of Materials Chemistry* **2007**, *17*, 4914-4918.

- (18) Chung, P. W.; Kumar, R.; Pruski, M.; Lin, V. S. Y. *Advanced Functional Materials* **2008**, *In Press*.
- (19) Topal, M. D. *Biochemistry* **1984**, *23*, 2367-72.
- (20) Hoffmann, G. R.; Calciano, M. A.; Lawless, B. M.; Mahoney, K. M. *Environmental and Molecular Mutagenesis* **2003**, *42*, 111-121.
- (21) Bardosova, M.; Tredgold, R. H. *Journal of Materials Chemistry* **2002**, *12*, 2835-2842.
- (22) Mornet, S.; Vasseur, S.; Grasset, F.; Duguet, E. *Journal of Materials Chemistry* **2004**, *14*, 2161-2175.
- (23) Hu, S.-H.; Liu, T.-Y.; Huang, H.-Y.; Liu, D.-M.; Chen, S.-Y. *Langmuir* **2008**, *24*, 239-244.
- (24) Babincova, M.; Cicmanec, P.; Altanerova, V.; Altaner, C.; Babinec, P. *Bioelectrochemistry* **2002**, *55*, 17-19.

CHAPTER 5. GENERAL CONCLUSION

The research that I accomplished during last six years is presented in this dissertation in chronological order. The original goal of this doctoral research was to develop a mesoporous silica material based targeted drug delivery system which is capable of releasing drug in response to specific stimulus.

Prior to the beginning of my research work, few major types of delivery systems were known in the field of controlled drug delivery for cancer therapeutics. Some of those had the stimuli-responsive controlled release property but lacked targeting property at the same time. Few other systems contained the site directing ability but lacked 'zero release' property, which is the most important criterion for a chemotherapy agent. My first project involved the fabrication of magnetic nanoparticles capped mesoporous silica nanomaterial that could store drug molecules and in absence of any stimuli, drugs were not able to come out from the system, thus fulfilling the 'zero release' criterion. Being capped by magnetic nanoparticles, the entire mesoporous assembly became magnetic and therefore the system was successfully targeted to a specific site by an external magnetic field. As, the system was designed to deliver guest molecules in response to a cancer cell produced antioxidant stimulus, we demonstrated that the magnetic drug delivery system was able to deliver the loaded guest molecules inside a cancer cell line upon internalization by those cells.

We also demonstrated that the cancer cell lines became magnetic once the cells took up Magnet-MSNs by endocytosis. Using an external magnet, it was even possible to maneuver the cells containing Magnet-MSNs. Apart from establishing the intracellular release of fluorescent guest molecules from Magnet-MSNs, we also showed the antioxidant

stimuli-responsive *in vitro* release of a mutagenic drug 9-aminoacridine using the same system. The *in vivo* application of the drug loaded Magnet-MSNs led to the enhanced growth inhibition of cancer cell lines. The growth inhibition was also shown to be unaffected by the presence of any strong external magnetic field.

Although, the Magnet-MSN systems that were developed during the earlier part of my doctoral research showed stimuli-responsive property; it failed to show any controlled-release behaviour once the system went inside the cells. In other words, we did not have any control on the release of guest molecules from Magnet-MSNs once the materials were internalized by the cells. In this context, I developed a novel controlled-release delivery system where the delivery of guest molecules can be precisely controlled by an external magnetic field. A thermo-responsive polymer coated MSN system attached with magnetic nanoparticles had been developed such that a thermal stimulus could be utilized to release stored guest molecules from the delivery system. The principle of hyperthermia was used to produce thermal energy by exposing the attached magnetic nanoparticles in an alternating magnetic field. The high frequency alternating magnetic field served as 'true' trigger to induce the drug release as well as to manipulate the amount of drug release. This novel system can be viewed as a primary approach towards magnetic field guided chemotherapy treatments, where the extent of drug release can be controlled by an external magnetic field as required by the particular treatment. The *in vivo* applications of this thermo-responsive delivery system offer a vast area of new research.

Finally, I can conclude that in this dissertation I have reported novel nanomaterial based targeted delivery systems that can provide pathways to develop new generations of cancer chemotherapy techniques in the field of biomedicine.